Cell Biology

A stable microtubule bundle formed through an orchestrated multistep process controls quiescence exit

Reviewed Preprint

Published from the original preprint after peer review and assessment by eLife.

About eLife's process

Reviewed preprint version 1
September 1, 2023 (this version)

Sent for peer review
June 30, 2023

Posted to preprint server
May 3, 2023

Damien Laporte, Aurélie Massoni-Laporte, Charles Lefranc, Jim Dompierre, David Mauboules, Emmanuel T. Nsamba, Anne Royou, Lihi Gal, Maya Schuldiner, Mohan L. Gupta Jr, Isabelle Sagot

Univ. Bordeaux, CNRS, IBGC, UMR 5095, Bordeaux, France • Genetics, Development, and Cell Biology, Iowa State University, Ames, IA 50011, USA • Department of Molecular Genetics, Weizmann Institute of Science, Rehovot, Israel

Abstract

Cells fine-tune microtubule assembly in both space and time, to give rise to distinct edifices with specific cellular functions. In proliferating cells, microtubules are highly dynamics, yet, proliferation cessation often lead to their stabilization. One of the most stable microtubule structures identified to date is the nuclear bundle assembled in yeast quiescent cells. In this report, we characterize the original multistep process driving the assembly of this structure in an AuroraB/Ipl1-dependent mechanism. This process follows a precise temporality that relies on the sequential actions of kinesin-14, kinesins-5 and involves both microtubule-kinetochore and kinetochore-kinetochore interactions. Upon quiescence exit, the microtubule bundle disassembles via a cooperative process involving the Kinesin-8 and its full disassembly is required to authorize cells re-entry into proliferation. Overall, our study not only provides the first description, at the molecular scale, of the entire life cycle of a stable microtubule structure *in vivo*, but also sheds light on its function as a sort of “checkpoint” for cell cycle resumption.

eLife assessment

This work presents **important** insights regarding the mechanism underlying the assembly, maintenance, and disassembly of a very stable microtubule-based structure, termed quiescent-cell nuclear microtubule (Q-nMT) bundle, formed in quiescent yeast cells to ensure cell survival and viability. Some of the evidence is **solid**, but some of the major claims are only **incompletely** supported and require additional analyses using state-of-the-art methodology and more precise descriptions.

Introduction

Microtubules (MT) are hollow cylindrical polymers assembled by the non-covalent interaction of α- and β-tubulin heterodimers. MTs are generally nucleated at MT organizing centers (MTOC) by a ɣ-tubulin complex (ɣ-TuC) that acts as a template and stabilizes the so-called MT "minus-end" (Liu et al., 2021; Roostalu and Surrey, 2017; Sanchez and Feldman, 2017; Thawani and Petry, 2021). At the opposite end, the "plus-end" (+end), MTs elongate by the addition of GTP tubulin. The β-tubulin bound GTP is hydrolyzed and stable but transient GDP + Pi intermediates are generated in the region immediately trailing the growing +end. A subsequent Pi release favors MT depolymerization that can be rescued by *de novo* GTP-tubulin addition (Cleary and Hancock, 2021; Gudimchuk and McIntosh, 2021). As such, MTs alternate periods of growth and shrinkage, a behavior called dynamic instability (Mitchison and Kirschner, 1984). *In vivo*, a profusion of MT associated proteins (MAPs) regulate MT length and dynamics (Bodakuntla et al., 2019; Goodson and Jonasson, 2018). Besides, MTs are often assembled from multiple tubulin variants or isotypes, and modified by a cohort of post-translational modifications that modulate MT dynamics directly or by influencing the recruitment of MAPs (Janke and Magiera, 2020; Roll-Mecak, 2020). Other MAPs organize MTs into high-ordered edifices either by cross-linking MTs or by connecting them with cellular structures such as membranes, chromosomes or components of the actin cytoskeleton (Bodakuntla et al., 2019; Meiring et al., 2020). Cells fine-tune these mechanisms both in space and in time to give rise to distinct MT architectures with specific function.

In proliferating cells, MT dynamic is crucial for their functions. It allows exploring the cell volume searching for structures to "capture", like centromeres during mitosis, or to exert pushing or pulling forces required for various cellular processes such as cell migration or morphogenesis (Heald and Khodjakov, 2015; Kirschner and Mitchison, 1986). Yet, the MT cytoskeleton can extensively rearrange and assemble more stable MT structures, notably when cells change fate (Meiring et al., 2020; Röper, 2020). For example, in terminally-differentiated cells, such as epithelial cells, cardiomyocytes or neurons, stable MT networks make up the majority, and ensure critical cellular functions such as cell shape maintenance or long-distance intra-cellular transport (Baas et al., 2016; Muroyama and Lechler, 2017). Defects in MT stabilization are at the origin of many human pathologies, including neuro-degenerative diseases and ciliopathies (Anvarian et al., 2019; Wheway et al., 2018). Effectors responsible for MT stabilization have been actively searched for since the 1980's. In mammals, the involvement of specific MAPs such as Tau, MAP2, MAP6 and PRC1, or tubulin post-translational modifications have been extensively studied. While their contributions to MT stabilization are central and undisputable, their sole actions do not fully explain the observed levels of MT stability in many types of non-dividing cells (Hahn et al., 2019).

For years, yeast species have been instrumental in deciphering mechanisms that regulate MT dynamics in eukaryotes. While proliferating yeast cells display a dynamic MT network (Winey and Bloom, 2012), proliferation cessation goes with the formation of dramatically stable MT structures in both *S. cerevisiae* and *S. pombe* (Laporte and Sagot, 2014; Laporte et al., 2013, 2015). Upon quiescence establishment, *S. cerevisiae* assemble a bundle composed of stable parallel MTs, hereafter called Q-nMT bundle, for Quiescent-cell nuclear Microtubule bundle, that emanates from the nuclear side of the spindle pole body (SPB), the yeast equivalent of the centrosome. The Q-nMT bundle spans the entire nucleus and relocalizes kinetochores and centromeres that remain attached to its MT +ends (Laporte and Sagot, 2014). Since MTs embedded into the Q-nMT bundle are not all of the same length, they confer to the structure a typical arrow shape. When cells exit quiescence, the Q-nMT bundle depolymerizes and, by pulling the attached centromeres back to the SPB, allows the recovery of the typical Rabl-like configuration of chromosomes found in G1 yeast cells (Jin et al., 1998). The molecular mechanisms underlying the formation of this peculiar stable MT structure and its physiological

function(s) are not understood. Yet, cells impaired for Q-nMT bundle formation have a compromised survival rate in quiescence and a drastically reduced fitness upon cell cycle re-entry (Laporte and Sagot, 2014; Laporte et al., 2013, 2015).

Here, we demonstrate that the Q-nMT bundle formation is a multistep process that follows a precise temporal sequence. The first step requires the kinesin-14 Kar3, its regulator Cik1 and the EB1 homolog Bim1, and leads to the formation of a short (≈ 1 µm) and stable bundle that resembles a half mitotic spindle. Importantly, in this first step, MT polymerization and stabilization are coupled. In a second step, additional MTs polymerize from the SPB, elongate, and are zipped to pre-existing ones in a Cin8/kinesin-5 dependant manner. The full Q-nMT bundle stabilization is established in a third and last step that requires the kinesin-5 Kip1. Our observations further indicate that Q-nMT bundle assembly requires not only MT-kinetochore attachment but also inter-kinetochore interactions. Finally, we show that, upon quiescence exit, the Q-nMT bundle disassembles from its +ends, where each MT depolymerizes in coordination with its neighbors, via the action of the depolymerase Kip3, a member of the kinesin-8 family. A complete Q-nMT bundle disassembly is required to authorize cells re-entry into the proliferation cycle. Overall, this study describes for the first time the entire life cycle of a MT structure from the molecular mechanisms involved in its formation and stabilization to its disassembly and further reveals that this atypical quiescent specific structure acts as a sort of “checkpoint” for cell cycle resumption upon quiescence exit.

Results

The Q-nMT bundle formation is a three-step process

To investigate whether the Q-nMT bundle was stable by default, *i.e.* intrinsically stable, or assembled as a dynamic structure and then stabilized, we quantified Q-nMT bundle length (**Fig. 1A**) and thickness (**Fig. 1B**) upon quiescence establishment following carbon source exhaustion. We found that the Q-nMT bundle assembly was a 3-step process. In an initial phase (phase I), MTs elongated from the SPB to reach ≈0.8 µm. The number of these so-called phase I-MTs was about the same as in a mitotic spindle (see inset of **Fig. 1B** and Sup. Fig. 1A). Importantly, phase I-MTs are resistant to nocodazole (Noc), a MT poison that causes dynamic MT depolymerization, indicating that their stabilization was concomitant with their polymerization (**Fig. 1A-B**). In a second phase, that started ≈10h after glucose exhaustion, additional MTs emerged from the SPB (phase II-MTs) and elongated along phase-I MTs, approximatively doubling the thickness of the phase I MT bundle (**Fig. 1B** and Sup **Fig. 1A**). At this stage, the tip of the newly elongated MTs were instable (**Fig. 1A-B**). Full Q-nMT bundle stabilization was reached ≈48h after glucose exhaustion (phase III), as Noc treatment affected neither Q-nMT bundle length nor its thickness (**Fig. 1A-B** and Sup. Fig. 1B). Another way to shed light on the Q-nMT bundle formation steps was to plot Q-nMT bundle width as a function of length for each individual cells before and after Noc treatment (**Fig. 1C**).

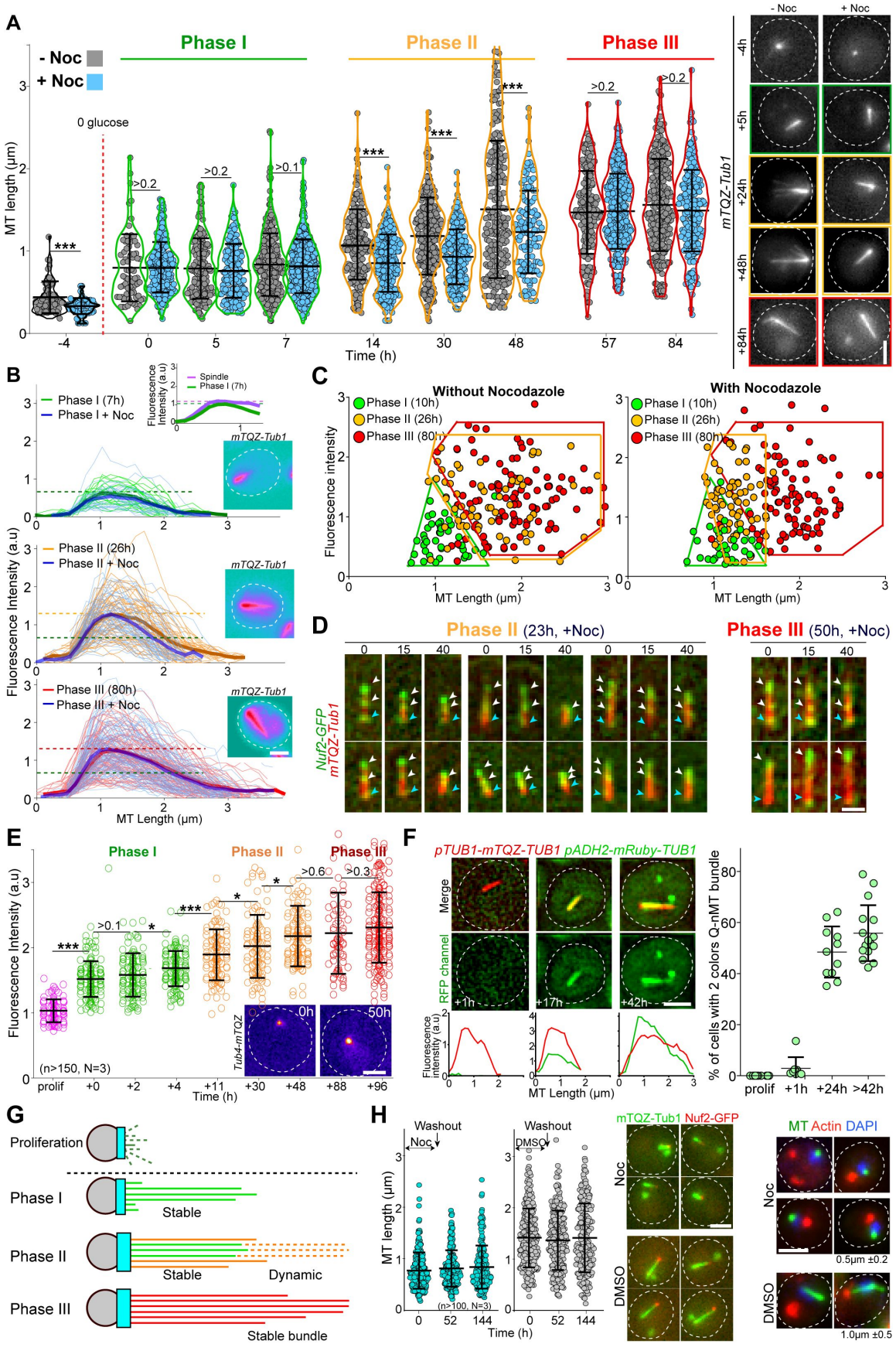
A
Phase I
Phase II
Phase III
- Noc
+ Noc
0 glucose
MT length (µm)
Time (h)
mTQZ-Tub1
B
Phase I (7h)
Phase I + Noc
Phase II (26h)
Phase II + Noc
Phase III (80h)
Phase III + Noc
Spindle
Fluorescence Intensity (a.u)
MT Length (µm)
C
Without Nocodazole
With Nocodazole
Fluorescence intensity
MT Length (µm)
D
Phase II (23h, +Noc)
Phase III (50h, +Noc)
Nuf2-GFP
mTQZ-Tub1
E
Tub4-mTQZ
(n>150, N=3)
F
pTUB1-mTQZ-TUB1 pADH2-mRuby-TUB1
Merge
RFP channel
% of cells with 2 colors Q-nMT bundle
G
Proliferation
Stable
Dynamic
Stable bundle
H
Washout
Noc
DMSO
(n>100, N=3)
mTQZ-Tub1 Nuf2-GFP
MT Actin DAPI
0.5µm ±0.2
1.0µm ±0.5

Figure 1

The formation of the Q-nMT bundle is a three-step process.

(A) Nuclear MT length in WT cells expressing mTQZ-Tub1, before (grey) or after a 15 min Noc treatment (blue) upon entry into quiescence.

(B) MT fluorescence intensity was used as a proxy of Q-nMT bundle width in WT cells expressing mTQZ-Tub1; thin line: intensity of an individual cell; bold line: mean intensity; n>60 for each phase. Mean intensity measurement for half pre-anaphase mitotic spindles (purple) phase I (green), phase II (orange) or phase III (red) Q-nMT bundle. To help comparison, in each graph, the dash line indicate the mean intensity in half pre-anaphase mitotic spindle. Representative cells are shown (images in pseudo-colors).

(C) Morphometric Q-nMT bundle property distribution (length and width) in each phase before and after a 15 min Noc treatment in WT cells expressing mTQZ-Tub1.

(D) Single WT cells expressing mTQZ-Tub1 (red) and Nuf2-GFP (green) in phase II (23h) or phase III (50h) were deposited on an agarose pad containing Noc and imaged. Blue arrowheads: SPB; white arrows: Nuf2-GFP clusters; time is in min after pad deposition.

(E) Tub4-mTQZ fluorescence intensity measured at the SPB upon entry into quiescence. Representative cells are shown (images in pseudo-colors). Bar is 1µm

(F) WT cells expressing mTQZ-Tub1 (red) under the *TUB1* promoter and mRuby-Tub1 (green) under the *ADH2* promoter. Representative cells at the indicated time after glucose exhaustion and the associated line-scans are show. The graph shows the percentage of cells harboring both mTQZ and mRuby fluorescence along the Q-nMT bundle. Each circle is the percentage obtained for an independent cell culture, n>200).

(G) Schematic of the Q-nMT bundle formation. During phase I, stable MTs (green) elongate from the SPB (in grey). During phase II, new MTs (orange) elongated from the SPB and are stabilized along the phase I MTs, but stay dynamic when longer than phase I MTs. In the meantime, Tub4 (blue) increases at the SPB (grey). After phase III, all MTs are stable (red).

(H) Upon glucose exhaustion, WT cells expressing mTQZ-Tub1 (green) and Nuf2-GFP (red) were pulsed treated with Noc (blue) or DMSO (grey) for 24 h. Noc or DMSO were then chased using carbon exhausted medium and cells were imaged. Representative images of cells 2 d after the chase are shown. Right panel: same experiment done in WT prototroph cells and representative images of cells 4 d after the chase are shown. Tubulin (green) was detected by immunofluorescence, actin (red) by phalloidin and DNA (blue) with DAPI. The mean Q-nMT bundle length (±SD) in the population is indicated.

In A, C, E an H, each circle corresponds to a single cell. In A, E, F and H mean and SD are shown, and unpaired T-test p-values are indicated; ***: p-value<10^{-5}. In A, D, F and H bar is 2µm.

To confirm the above multistep process, we first followed Nuf2-GFP, a protein that localize at the MT +end. In phase I, Nuf2-GFP signal relocates from SPB to the distal part of elongating Q-nMT bundles (Sup. Fig. 1D). In phase II, when cells were treated with Noc, the Nuf2-GFP signal followed depolymerizing MTs (**Fig. 1D**), testifying for the instability of phase II MTs. By contrast, the Nuf2-GFP signal remained immobile in phase III, when cells have fully stabilized Q-nMT bundles (**Fig. 1D**). Second, we measured the γ-tubulin (Tub4) signal at the SPB and found that Tub4 started accumulating at the SPB at the onset of phase I to reach a plateau at the end of phase II (**Fig. 1E** and Sup. Fig. 1E). Interestingly, the amount of Tub4 at the SPB was proportional to the thickness of the Q-nMT bundle (Sup. Fig. 1F). Finally, in order to confirm the two waves of MT

elongation, we developed a strain expressing mTQZ-Tub1 from the endogenous TUB1 promoter and mRuby-TUB1 under the ADH2 promoter, a promoter that is active only after glucose exhaustion. We observed that mRuby-TUB1 was incorporated into the Q-nMT bundle only after phase I (**Fig. 1F** and Sup. Fig. 1G) confirming the existence of a second wave of MT elongation in phase II. All the above information lead us to propose the model presented in **Fig. 1G** (see figure legend).

Q-nMT bundle formation is an active process regulated in time

Increasing viscosity of the cytoplasm was shown to dampen MT dynamics (Molines et al., 2022). Upon quiescence establishment, yeast cells experience a fluid phase to solid-like transition (Munder et al., 2016; Joyner et al., 2016) and an acidification (Jacquel et al., 2021) that could contribute to Q-nMT bundle formation. Several evidences indicate that these changes in physico-chemical properties are not involved in Q-nMT formation. First, 4-day-old quiescent cells can simultaneously display both dynamic cytoplasmic MTs (cMT) and a stable Q-nMT bundle (Sup. Fig. 1H and (Laporte et al., 2013)). Second, when we mimicked a fluid phase to solid like transition in proliferating cells by artificially dropping the pH, no stable MTs were observed, while F-actin aggregation was induced (Sup. Fig. 1I) as expected from (Peters et al., 2013). Third, 2-day-old quiescent cells displaying a phase III Q-nMT bundle were able to grow *de novo* dynamic MTs after a pulsed-chase Noc treatment (Sup. Fig. 1J).

If Q-nMT bundle formation was solely depending on physico-chemical changes, this structure should be able to assemble in late quiescence. By treating cells with Noc upon glucose exhaustion, we managed to prevent Q-nMT bundle formation in early quiescence (**Fig. 1H**). Strikingly, when the drug was washed out 24 h later, no Q-nMT bundle assembled, even several days after Noc removal (**Fig. 1H**). We verified that these cells did enter quiescence as they assembled actin bodies (**Fig. 1H**, right panel), another quiescent cell specific structure (Sagot et al., 2006). This experiment strongly suggests that Q-nMT formation is an active process induced by a transient signal emitted upon glucose exhaustion.

Mutants that cannot assemble Q-nMT bundle have a reduced viability in quiescence and a decreased capacity to form colonies upon quiescence exit (Laporte et al., 2013). To establish a causal link between the absence of Q-nMT bundle and the above phenotypes, we took advantage of our ability to prevent conditionally Q-nMT bundle formation in WT cells using early Noc treatment. We demonstrated that in the absence of Q-nMT bundle, both prototroph and auxotroph WT cells loose viability in quiescence and that survivors had a reduced capacity to generate a progeny upon quiescence exit (Sup. Fig. 1K). This reinforce the idea that the Q-nMT bundle is required for cell survival upon chronological aging.

Tubulin steady state level and Tub3 isoform are critical for Q-nMT bundle formation

We then focused on deciphering the molecular mechanisms involved in Q-nMT bundle formation. Yeast cells express two α-tubulin isotypes, Tub1 and Tub3. In proliferating cells, Tub1 make up the majority (Aiken et al., 2019; Nsamba et al., 2021; Schatz et al., 1986). In 4-day-old cells, both isoforms were embedded into the Q-nMT bundle (**Fig. 2A** and Sup. Fig. 2A). As Tub3 stabilizes MTs *in vitro* (Bode et al., 2003), it may be key for Q-nMT bundle formation in quiescence. To test this hypothesis, we first analyzed the phenotype of *tub3Δ* cells. In phase II, *tub3Δ* cells displayed short MT bundles that were highly sensitive to Noc. In phase III, no MT bundle could be detected (**Fig. 2B**). Thus in this mutant, MT bundles assembled during phase I were not stable and ultimately collapsed. Yet, in *tub3Δ* cells, the steady state amount of α-tubulin is significantly decreased (Sup. Fig. 2B and (Nsamba et al., 2021)). Thus, the amount of α-tubulin, but not Tub3 itself, could be important for Q-nMT bundle formation. Indeed, mutants impaired for α- and β-tubulin folding, such as the prefolding complex mutants *pac10Δ*, *gim3Δ* or *yke2Δ*, or for tubulin

heterodimer formation such as *pac2Δ*, or for β-tubulin folding, such as *cin2Δ* or *cin4Δ*, all of which displaying a decreased amount of tubulin, were unable to assemble a Q-nMT bundle (Sup. Fig. 2C-D).

To identify the role of Tub3 *per se*, we took advantage of the "*Tub1-only*" mutant in which the *TUB3* gene was replaced by the *TUB1* gene at the *TUB3* locus. This mutant only expresses Tub1 and displays an α-tubulin level similar to WT (Sup. Fig. 2B and (Nsamba et al., 2021)). We found that "*Tub1-only*" cells display shorter but stable Q-nMT bundles in phase III (**Fig. 2C**). Interestingly, "*Tub1-only*" Q-nMT bundles were thinner than WT Q-nMT bundles (**Fig. 2D**). Overall, these data indicate Tub3 is involved in MT elongation in phase II.

Kinetochores are critical for phase I but dispensable for the maintenance of Q-nMT bundles

Kinetochore components are enriched at the Q-nMT bundle +end ((Laporte et al., 2013) and Sup **Fig. 3A**). We thus wondered if kinetochore-MT attachment could play a role in Q-nMT bundle formation. First, we disrupted kinetochore-MT attachment upon phase I using the well-established *ndc80-1* allele (Cheeseman et al., 2006; DeLuca et al., 2018; Wigge et al., 1998). As shown in **Fig. 3A**, no Q-nMT bundles were detected in *ndc80-1* cells shifted to 37°C at the onset of quiescence entry. Second, we focused on the chromosomal passenger complex (CPC: Bir1/Survivin, Sli15/INCENP, Nbl1/Borealin and Ipl1/Aurora B), a complex known to regulate kinetochore-MT attachment dynamics (Cairo and Lacefield, 2020). We found that upon quiescence entry, Ipl1 inactivation impeded MT bundle formation (**Fig. 3B**). While we could not detect Ipl1 and Ndc1 in quiescent cells, we found that Sli15-GFP and Bir1-GFP localized along the Q-nMT bundle with an enrichment at the Q-nMT bundle +end (**Fig. 3C**). The deletion of Sli15 did not affect Q-nMT bundle (Fig. Sup. 3E). However, in 4-days old *bir1Δ* cells, Q-nMT bundle length were slightly shorter and not fully stabilized (**Fig. 3D**). Finally, we investigated the involvement of Bim1, a MT +end binding protein that plays a role in kinetochore MT-end on attachment (Dudziak et al., 2021; Thomas et al., 2016). We have previously shown that Bim1 localizes all along the Q-nMT bundle but that its deletion has no impact on Q-nMT bundle formation even in the presence of Noc ((Laporte et al., 2013) and **Fig. 3D**). Interestingly, the amount of Bim1 was correlated with tubulin incorporation during Q-nMT bundle formation (Sup **Fig. 3D**). When we combined *bim1Δ* with *bir1Δ*, cells hardly assembled MT structures that vanished after Noc treatment (**Fig. 3D**). This demonstrates that in the absence of Bim1, Bir1 was critical for Q-nMT bundle stabilization in phase I. A similar phenotype was observed with *SLI15* deletion (Sup **Fig. 3E**). Interestingly, the viability of *bim1Δ bir1Δ* cells in quiescence was drastically reduced (Sup **Fig. 3G**). Together, these experiments show that kinetochore-MT attachments are critical for the initiation of Q-nMT bundle assembly.

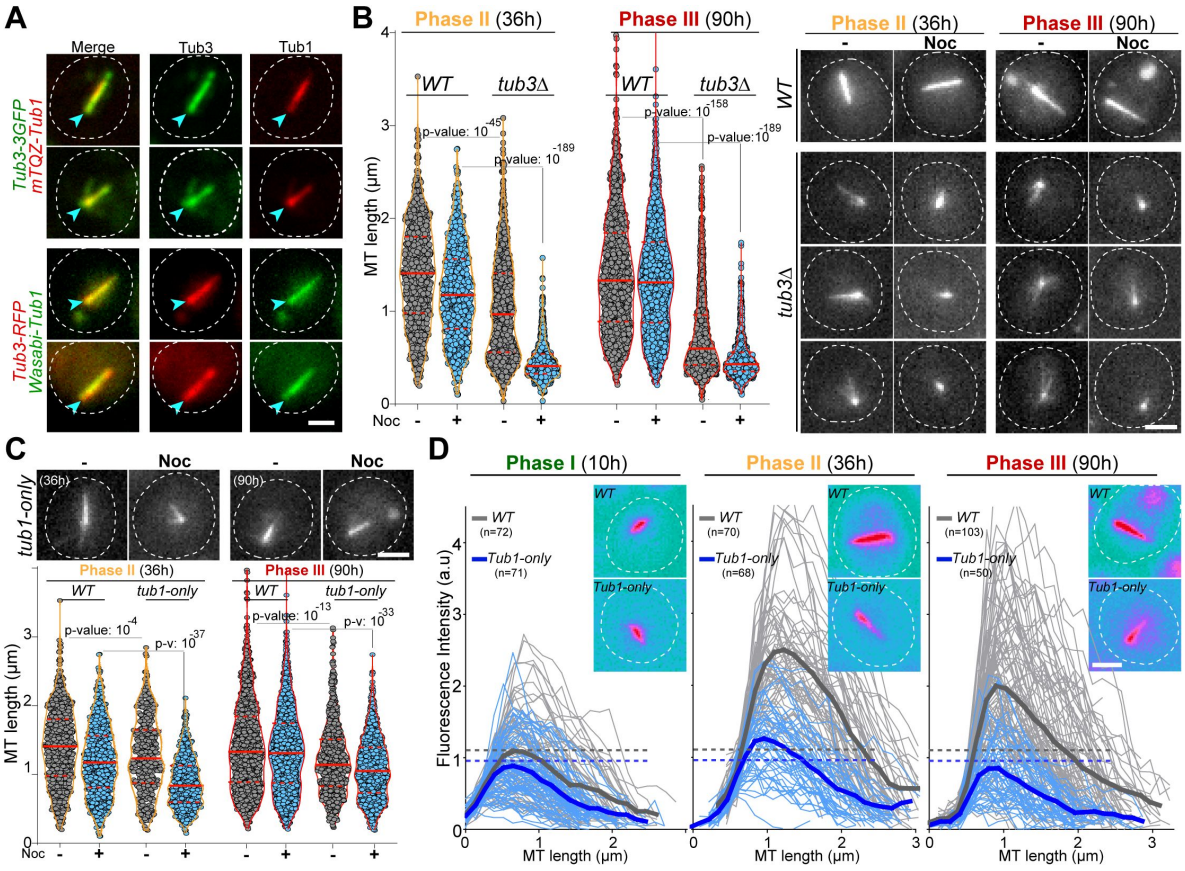

Figure 2

Q-nMT bundle formation is influenced by the alpha-tubulin amount and isoform

(A) WT cell (4 d) expressing either Tub3-3GFP (green) and mTQZ-Tub1 (red, top panel) or Tub3-RFP (red) and mWasabi-Tub1 (green, bottom panel). Blue arrowheads point to SPB.
(B) Nuclear MT length in WT and *tub3Δ* cells expressing mTQZ-Tub1, 36 h (phase II, yellow) and 90 h (phase III, red) after glucose exhaustion, treated 15 min (blue) or not (grey) with Noc. Representative images are shown on the right.
(C) Nuclear MT length in WT and *Tub1-only* cells expressing mTQZ-Tub1, 36 h (phase II, yellow) and 90 h (phase III, red) after glucose exhaustion, treated 15 min or not with Noc. Representative images are shown on top.
(D) Fluorescence intensity along the Q-nMT bundle in WT (grey) and *Tub1-only* (blue) cells expressing mTQZ-Tub1 grown for 10 h (phase I), 36 h (phase II), and 90 h (phase III). Thin lines indicate individual cells fluorescence intensity and bold lines, the mean intensity. Dashed lines indicate the maximal mean fluorescence intensity measured in phase I.
In B and C, each circle corresponds to a single cell. MT mean length, SD, and unpaired T-test p-value are indicated. In all panels, bar is 2µm.

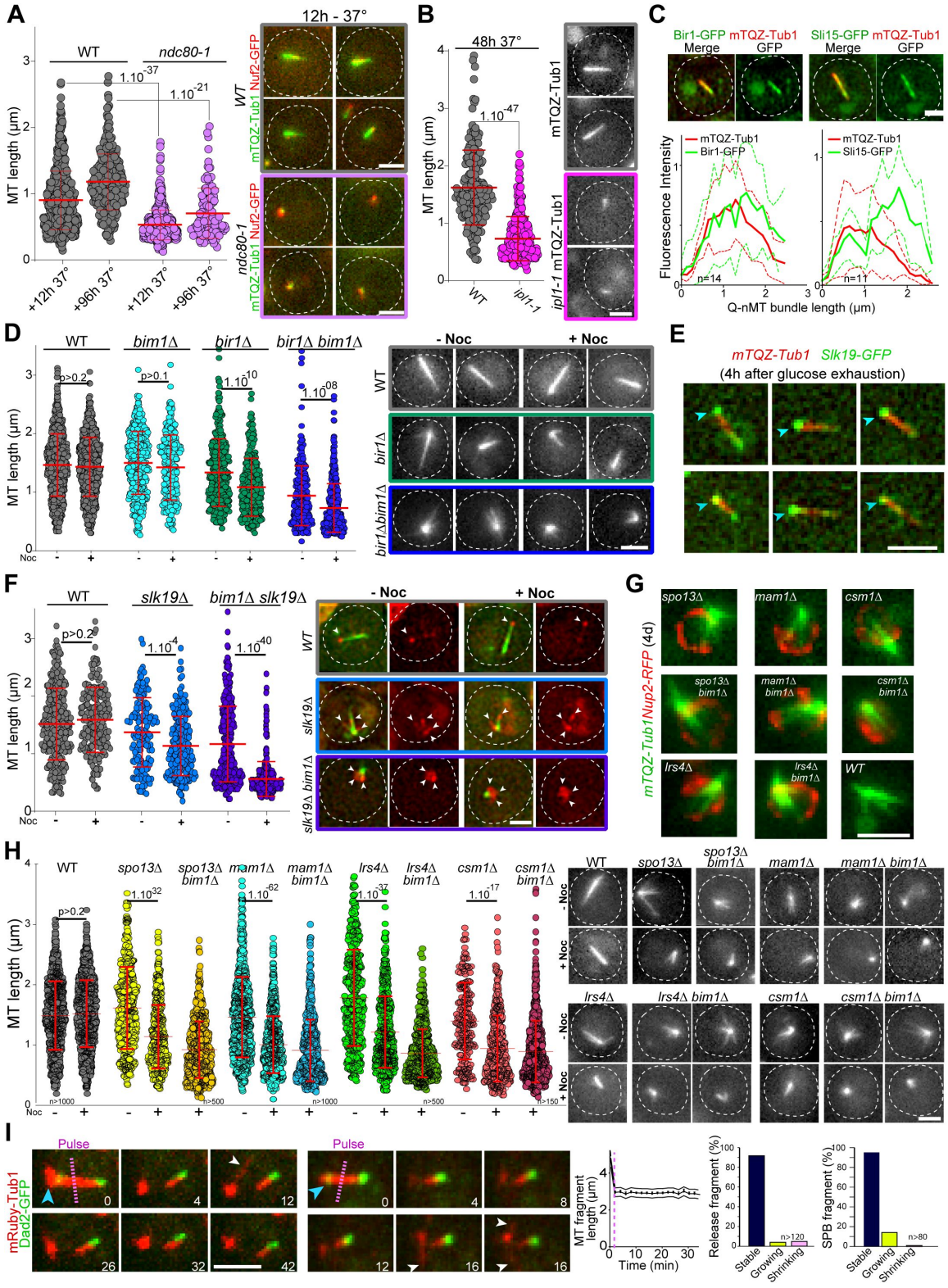
A
12h - 37°
WT
ndc80-1
MT length (µm)
+12h 37°
+96h 37°
mTQZ-Tub1 Nuf2-GFP
B
48h 37°
ipl1-1
mTQZ-Tub1
C
Bir1-GFP mTQZ-Tub1
Sli15-GFP mTQZ-Tub1
Merge
GFP
Fluorescence Intensity
Q-nMT bundle length (µm)
D
bim1Δ
bir1Δ
bir1Δ bim1Δ
- Noc
+ Noc
E
mTQZ-Tub1 Slk19-GFP
(4h after glucose exhaustion)
F
slk19Δ
bim1Δ slk19Δ
G
mTQZ-Tub1Nup2-RFP (4d)
spo13Δ
mam1Δ
csm1Δ
lrs4Δ
H
spo13Δ bim1Δ
mam1Δ bim1Δ
csm1Δ bim1Δ
lrs4Δ bim1Δ
I
Pulse
mRuby-Tub1
Dad2-GFP
MT fragment length (µm)
Time (min)
Release fragment (%)
SPB fragment (%)
Stable
Growing
Shrinking

Figure 3

Kinetochore-kinetochore interactions are required for Q-nMT bundle formation.

(A) Nuclear MT length distribution in WT (grey) and *ndc80-1* (violet) cells expressing mTQZ-Tub1 (green) and Nuf2-GFP (red), shifted to 37 °C upon glucose exhaustion for the indicated time and imaged after a 20 min Noc treatment. Representative cells shifted for 12 h at 37°C are shown.

(B) WT (grey) and *ipl1-1* cells (pink) expressing mTQZ-Tub1 were shifted upon glucose exhaustion to 37 °C for 48 h, and imaged after a 20 min Noc treatment. Representative cells are shown.

(C) WT cells (2 d) expressing mTQZ-Tub1 (red) and Bir1-GFP or Sli15-GFP (green) were imaged. Graphs show Bir1-GFP or Sli15-GFP fluorescence intensity along normalized Q-nMT bundles (plain and dash lines: mean and SD respectively).

(D) Nuclear MT length distribution in cells of the indicated genotype (4 d) expressing mTQZ-Tub1 treated or not with Noc. Representative cells are shown.

(E) WT cells expressing mTQZ-Tub1 (red) and Slk19-GFP (green) 4 h after glucose exhaustion. Blue arrowhead: SPB.

(F) Nuclear MT length distribution in cells of the indicated genotype (4 d) expressing mTQZ-Tub1 (green) and Nuf2-GFP (red) were imaged before or after Noc treatment. Representative cells are shown. White arrowheads point to Nuf2 dots.

(G) Cells of the indicated genotype (4 d) expressing mTQZ-Tub1 (green) and Nup2-RFP (red).

(H) Nuclear MT length distribution in cells of the indicated genotype (4 d) expressing mTQZ-Tub1 treated or not with Noc. Representative cells are shown.

(I) Length variation of nuclear MT bundle fragments after laser ablation (pink dash line) in cells expressing mRuby-TUB1 (red) and Dad2-GFP (green). Time is in min. Blue arrowhead: SPB, white arrowhead: cMT.

In A, B, D, F, and H, each circle corresponds to a single cell. Mean, SD, and unpaired T-test p-values are indicated (*: p-value <0.05, and ***: p-value $<10^{-6}$). Bar is 2 µm except in (I) where it is 1 µm.

We then hypothesized that inter-kinetochore interactions may stabilize the parallel MTs embedded into the Q-nMT bundle. To test this idea, we analyzed MT organization in s*lk19Δ* cells that are defective in kinetochore clustering (Richmond et al., 2013). In quiescence, Slk19 was enriched at both Q-nMT bundle extremities (**Fig. 3E**). s*lk19Δ* cells displayed shorter and thinner MT structures that were not stable, i.e. sensitive to Noc treatmant (**Fig. 3F**). Since Bim1 has been involved in kinetochore-kinetochore interaction, we combined s*lk19Δ* with *bim1Δ*. MT structures detected in s*lk19Δ bim1Δ* cells hardly reached ≈1 µm and vanished upon Noc treatment. In addition, kinetochores localized as a rosette around the SPB (**Fig. 3F**) and cell viability was strongly compromised (Sup. Fig. 3G). This demonstrates that in the absence of Bim1, Slk19 is strictly essential for MT bundling and stabilization in phase I. Furthermore, since kinetochores are known to be cross-linked by the monopolin complex (Mam1, Lrs4, Hrr25 and Csm1 (Corbett et al., 2010)) we analyzed the phenotype of *mam1Δ*, *lrs4Δ* and *csm1Δ* cells in quiescence. Most of them displayed short MT structures often arranged in a star-like array (**Fig. 3G-H**, Sup. Fig. 3F). As for Bir1 and Skl19, the combination of *bim1* deletion with monopolin disruption worsens MT structure length and stability (**Fig. 3H**) and the cell viability was strongly compromised (Sup. Fig. 3G).

Cells impaired for Spo13, a protein involved in monopolin recruitment to kinetochores (Lee et al., 2004) displayed a similar phenotype (**Fig. 3G-H**). Altogether, these experiments show that inter-kinetochore interactions are critical for Q-nMT bundle assembly.

Lastly, we investigated if kinetochore-MT interactions were required for Q-nMT bundle stability once it is formed. In 5-days old WT cells, we used a UV-pulsed-laser to break the Q-nMT bundle into two pieces (**Fig. 3I**). The presence of dynamic cMTs after laser ablation testified for cell viability (**Fig. 3I**). In most cases, the length of both the released fragment and the fragment attached to the SPB remained constant (**Fig. 3I**, Sup. Fig. 3H). By contrast, in proliferating cells, dynamic anaphase spindles promptly disassembled following a pulse-laser break (Sup. Fig. 3I). This demonstrates that once Q-nMT bundles are formed, they do not need MT-kinetochore interaction to be maintained. Accordingly, Ndc80 or Ipl1 inactivation in cells that are already in quiescence had no effect on the Q-nMT bundle maintenance (Sup. Fig. 3B-C). Importantly, the above experiment indicates that once formed, Q-nMT stability is established and maintained throughout its length.

Specific kinesins are required for each step of Q-nMT bundle formation

To go further in the deciphering of the molecular mechanism involved in Q-nMT bundle formation, we focused on kinesins. Kar3 is a kinesin that, in complex with its regulator Cik1, can generate parallel MT bundles from a MT organizing center (MTOC) both *in vitro* and in proliferative cells (Manning et al., 1999; Mieck et al., 2015; Molodtsov et al., 2016). In quiescence, we found that Kar3-3GFP localized at the SPB, but also as dots along the Q-nMT bundle (**Fig. 4A**). In 4 day-old *kar3Δ* cells, the majority of the detected MT structures were extremely short compared to WT (**Fig. 4B** and Sup **Fig. 4A**). Same results were obtained in *cik1Δ* but not in *vik1Δ* cells, which lack the alternate Kar3 regulators (**Fig. 4B**). Thus, the Kar3/Cik1 complex is required for phase I.

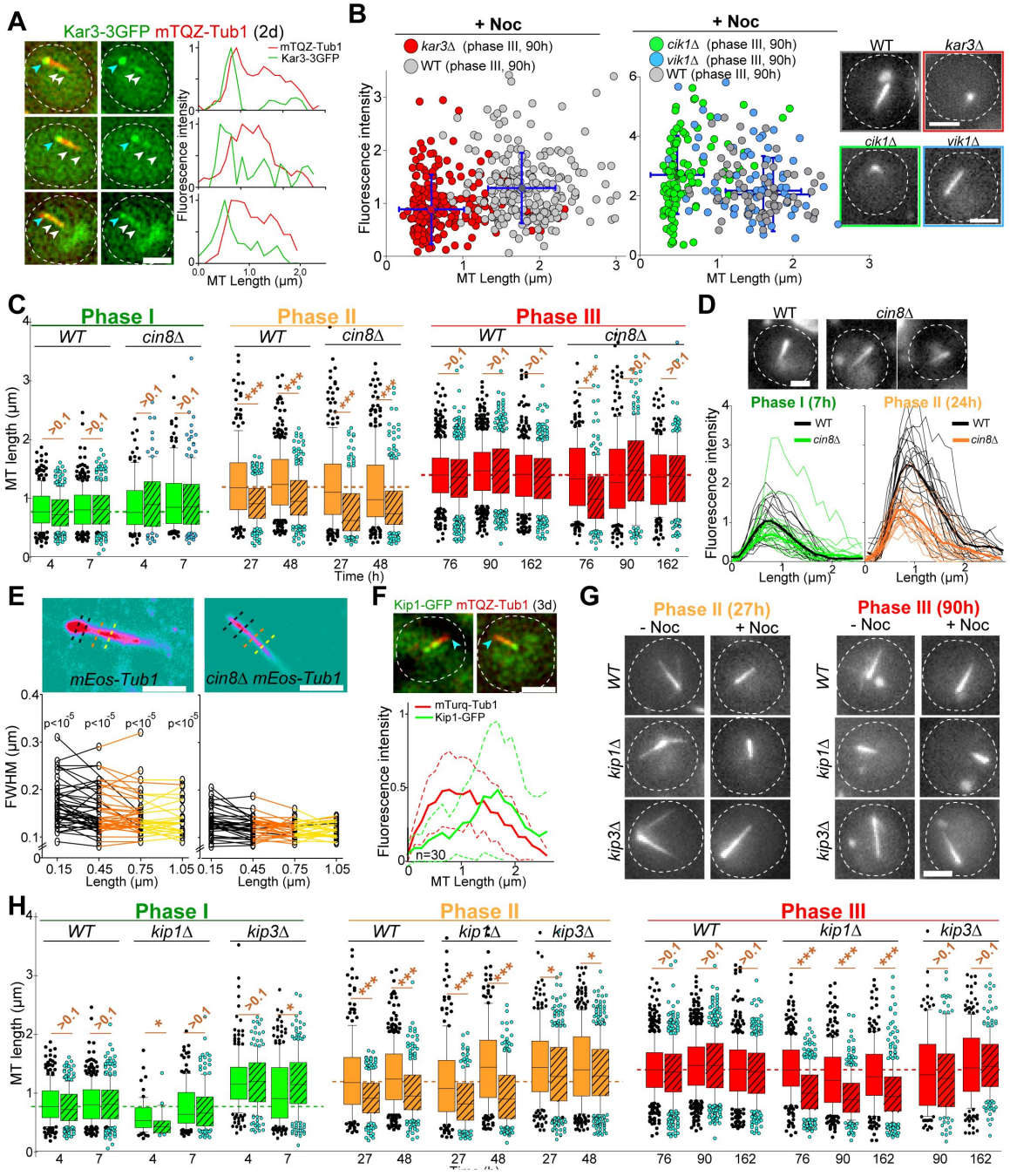
A
Kar3-3GFP mTQZ-Tub1 (2d)
mTQZ-Tub1
Kar3-3GFP
Fluorescence intensity
MT Length (µm)
B
+ Noc
kar3Δ (phase III, 90h)
WT (phase III, 90h)
Fluorescence intensity
MT Length (µm)
+ Noc
cik1Δ (phase III, 90h)
vik1Δ (phase III, 90h)
WT (phase III, 90h)
MT Length (µm)
WT
kar3Δ
cik1Δ
vik1Δ
C
Phase I
Phase II
Phase III
WT
cin8Δ
MT length (µm)
Time (h)
D
WT
cin8Δ
Phase I (7h)
Phase II (24h)
Fluorescence intensity
Length (µm)
E
mEos-Tub1
cin8Δ mEos-Tub1
FWHM (µm)
Length (µm)
F
Kip1-GFP mTQZ-Tub1 (3d)
mTurq-Tub1
Kip1-GFP
Fluorescence intensity
n=30
MT Length (µm)
G
Phase II (27h)
Phase III (90h)
- Noc
+ Noc
WT
kip1Δ
kip3Δ
H
Phase I
Phase II
Phase III
WT
kip1Δ
kip3Δ
MT length (µm)

Figure 4

Each phase of Q-nMT formation requires a specific kinesin.

(A) Images and corresponding line scans of WT cells (2 d) expressing Kar3-3GFP (green) and mTQZ-Tub1 (red).

(B) Morphometric Q-nMT bundle properties distribution in 4 d WT (grey), *kar3Δ* (red), *vik1Δ* (blue), *cik1Δ* cells (green) expressing mTQZ-Tub1 after Noc treatment. Blue crosses are SD. Each circle corresponds to an individual Q-nMT bundle. Representative cells are shown.

(C) Nuclear MT length distribution in WT and *cin8Δ* cells expressing mTQZ-Tub1 treated (dashed boxes) or not (plain boxes) with Noc.

(D) Fluorescence intensity along Q-nMT bundle in WT and *cin8Δ* cells expressing mTQZ-Tub1 7 h and 24 h after glucose exhaustion. Representative cells are shown.

(E) WT and *cin8Δ* cells expressing mEOS3.2-Tub1 were imaged using PALM (images are in pseudo-colors). Full width at half maximum (FWHM) was measured at the indicated distance from the SPB. Each line in the bottom graph corresponds to a single cell. P-value between WT and *cin8Δ* are indicated (unpaired T-test).

(F) WT cells (3 d) expressing Kip1-GFP (green) and mTQZ-Tub1 (red). Graphs show fluorescence intensity along normalized Q-nMT bundles (plain and dash lines: mean and SD respectively).

(G-H) Representative images and nuclear MT length distribution in WT, *kip1Δ* and *kip3Δ* cells expressing mTQZ-Tub1 treated (dashed boxes) or not (plain boxes) with Noc.

In C and H, *: p-value <0.05, and ***: p-value $<10^{-6}$ (unpaired T-test). Means and SD are indicated. In A, B, D, E, F and G, bar is 2 µm.

Cin8 is a Kinesin-5 that cross-links MTs (Bodrug et al., 2020; Pandey et al., 2021; Singh et al., 2018), and as such, could play a role in Q-nMT bundle stabilization. Cin8 was hardly detectable in quiescent cells (Sup. Fig. 4B) and *cin8Δ* cells assembled Q-nMT bundles that were thinner than in WT cells (**Fig. 4C-E**). Yet, these thinner bundles became stabilized in phase III (**Fig. 4C** and Sup. Fig. 4C-D). Overall, these results strongly suggest that Cin8 is required for phase II MT nucleation and/or elongation but not for stabilization in phase III.

Yeast have an additional Kinesin-5 called Kip1 (Fridman et al., 2013). In quiescence, most of the Kip1-GFP signal was observed at the Q-nMT bundle +end (**Fig. 4F**). In *kip1Δ* cells, phase I was slightly delayed and Q-nMT bundle were not stabilized in phase III (**Fig. 4G-H**), yet they were as thick as WT Q-nMT bundles (Sup. Fig. 4E). These data demonstrate that Kip1 is required for Q-nMT bundle stabilization in phase III. Of note, in phase I and II, Q-nMT bundles were slightly longer in cells deleted for the Kinesin-8 Kip3, a MT depolymerase ((Fukuda et al., 2014) **Fig. 4 G-H** and Sup. Fig. 4G) but were unaffected in cells deleted for Kip2, a kinesin that stabilizes cytoplasmic MTs ((Hibbel et al., 2015) Sup. Fig. 4F-G). Taken together our results demonstrate that each phase of Q-nMT bundle assembly involves specific kinesins.

Q-nMT bundle disassembly conditions SPB duplication/separation

Finally, we questioned the molecular mechanism of Q-nMT bundle disassembly upon quiescence exit. Cycloheximide prevented Q-nMT bundle disassembly indicating that this process requires *de novo* protein synthesis (**Fig. 5A**). We then measured Q-nMT bundle thickness upon depolymerization, and found that while Q-nMT bundles shortened, they did not get thinner (**Fig.**

5B). In agreement, Nuf2-GFP clusters found at the Q-nMT bundle +end moved back to the SPB while the Nuf2-GFP clusters localized in the middle of the structure remained immobile until they are reached by these later (Sup. Fig. 5 A). This shows that all the MT +ends did not start depolymerizing at the same time, and that longer MTs depolymerized first. This finding is in agreement with our model in which MTs are cross-linked all along the Q-nMT bundle length.

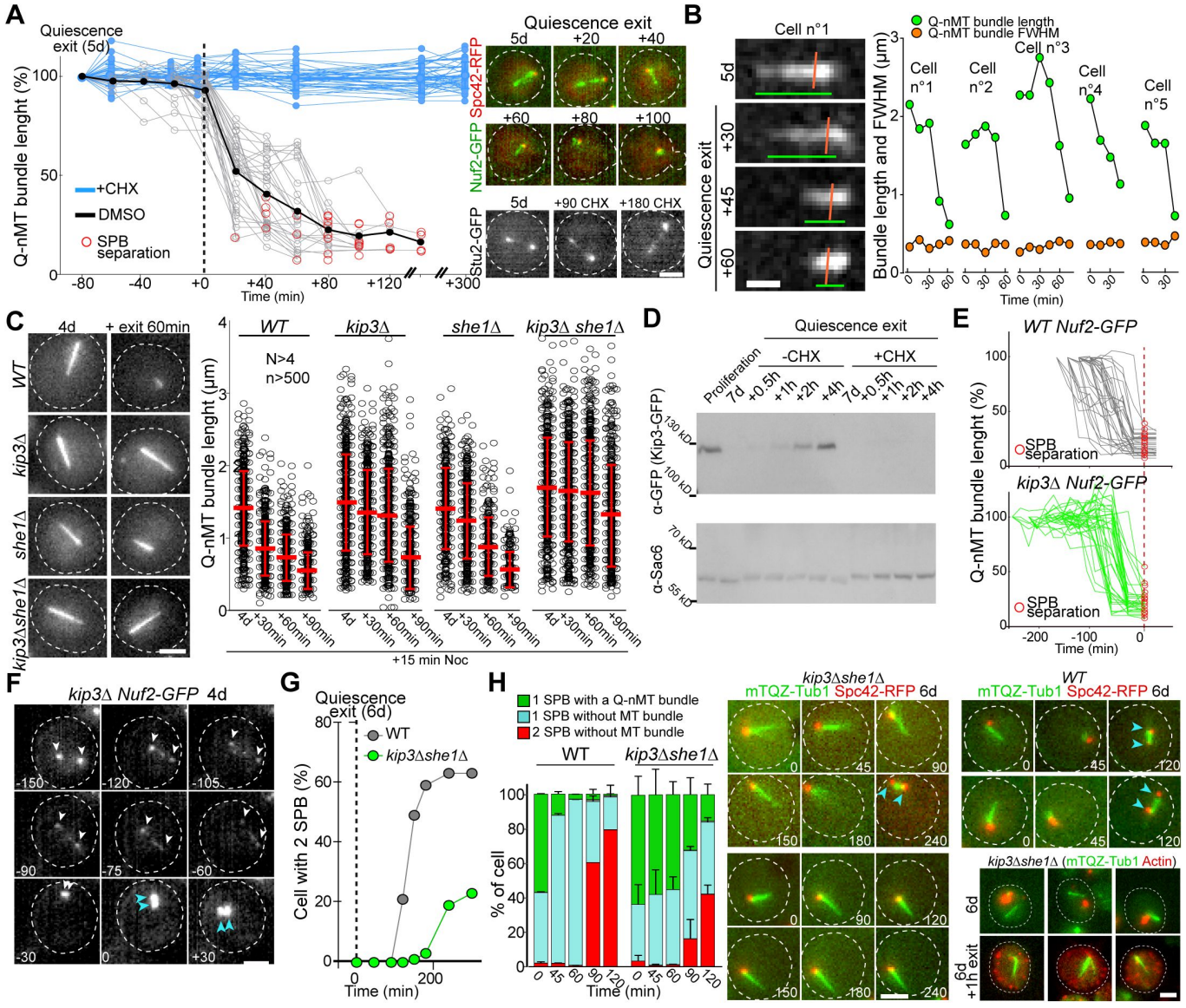
A
Quiescence exit (5d)
Q-nMT bundle lenght (%)
+CHX
DMSO
SPB separation
Time (min)
Quiescence exit
Spc42-RFP
Nuf2-GFP
Stu2-GFP
+90 CHX
+180 CHX
B
Cell n°1
Quiescence exit
Q-nMT bundle length
Q-nMT bundle FWHM
Bundle length and FWHM (µm)
C
WT
kip3Δ
she1Δ
kip3Δ she1Δ
N>4
n>500
Q-nMT bundle lenght (µm)
+15 min Noc
D
Quiescence exit
-CHX
+CHX
Proliferation
α-GFP (Kip3-GFP)
α-Sac6
E
WT Nuf2-GFP
kip3Δ Nuf2-GFP
SPB separation
F
kip3Δ Nuf2-GFP 4d
G
Quiescence exit (6d)
Cell with 2 SPB (%)
H
1 SPB with a Q-nMT bundle
1 SPB without MT bundle
2 SPB without MT bundle
% of cell
kip3Δshe1Δ mTQZ-Tub1 Spc42-RFP 6d
WT mTQZ-Tub1 Spc42-RFP 6d
kip3Δshe1Δ (mTQZ-Tub1 Actin)

Figure 5

Q-nMT bundle disassembly always occurs before SPB separation upon quiescence exit.

(A) WT cells expressing Spc42-RFP (red) and Nuf2-GFP (green) (5 d) were re-fed on an YPDA microscope pad. Individual Q-nMT bundles were measured in cells treated with CHX (blue, Stu2-GFP) or with DMSO alone (grey, Nuf2-GFP). Each line corresponds to an individual cell. For each cell, time was set to zero at the onset of MT bundle depolymerization (black dashed line).

(B) Q-nMT bundle length (green) and fluorescence intensity at full width half maximum (FWHM - orange) were measured upon quiescence exit in WT cells (5 d) expressing mTQZ-Tub1. Representative example of shirking Q-nMT bundle is shown on the left.

(C) Cells of the indicated genotype expressing mTQZ-Tub1 were grown for 4 d, and re-fed. Q-nMT bundle length was measured at the indicated time points, 15 min after a Noc treatment.

(D) Western blot (GFP antibodies) on total protein extracts from WT cells expressing Kip3-GFP grown for the indicated time. Sac6 was used as a loading control (Sac6 antibodies).

(E) WT and *kip3Δ* cells (5 d) expressing Nuf2-GFP were re-fed on an YPDA microscope pad. Each line corresponds to an individual cell. For each cell, time was set to zero at the onset of SPB separation.

(F) Representative images of *kip3Δ* cells expressing Nuf2-GFP upon quiescence exit. White arrowheads: Q-nMT bundle extremities.

(G) Percentage of cells expressing Spc42-mRFP1 with separated SPB as a function of time upon quiescence exit.

(H) WT and *kip3Δshe1Δ* cells (6 d) expressing Spc42-mRFP1 (red) and mTQZ-Tub1 (green) were re-fed on a YPDA microscope pad. Percentage of cells with a single or a duplicated SPB in the presence or absence of Q-nMT bundle were scored. Representative cells are shown. Right bottom panel: actin (phalloidin staining, red) in *kip3Δ she1Δ* cells (6 d) expressing mTQZ-Tub1 (green) before and 1 h after quiescence exit.

In F and H, blue arrowheads: SPB. In all panels, bar is 2 µm.

Since Kip3 is the only well-characterized yeast MT depolymerase, we studied Q-nMT bundle disassembly in *kip3Δ* cells and observed that it was drastically delayed (**Fig. 5C**), yet its overall depolymerization rate remained unaffected (Sup. Fig. 5B). In fact, we found that in WT cells, Kip3 needs to be resynthesized upon quiescence exit (**Fig. 5D**). We searched for proteins that could be involved in Q-nMT bundle disassembly together with Kip3. Among proteins required for mitotic spindle disassembly, we found that inactivation of *CDC14*, *CDC15*, *CDH1*, *DCC1* and *TOR1* had no effect on Q-nMT bundle disassembly, just as with the inactivation of Ipl1 or proteins involved in kinetochore-MT attachment (Sup. Fig. 5 C to F). The sole additional actor we found was She1, a dynein regulator (Bergman et al., 2012), which deletion strongly aggravated the *kip3Δ* phenotype (**Fig. 5C**). Thus, Q-nMT bundle disassembly does not rely on the canonical mitotic spindle disassembly machinery but, rather, specifically required Kip3 and She1.

Importantly, when we followed quiescence exit at the individual cell level, Q-nMT bundle depolymerization always preceded SPB duplication/separation (**Fig. 5A**) and thus, in both WT and in *kip3Δ* cells (**Fig. 5E, F**). In fact, when we impeded Q-nMT bundle disassembly using *kip3Δ she1Δ*, we found that SPB duplication was severely delayed (**Fig. 5G-H**, Sup. Fig. 5G-H). Importantly, *kip3Δ she1Δ* cells proliferated just like WT cells (Sup. Fig. 5G) and upon quiescence exit, these mutant cells disassembled actin bodies just as in WT cells (Sup. Fig. 5I), demonstrating

that *kip3Δ she1Δ* cells were not impaired in sensing quiescent exit signals. These observations indicate that Q-nMT bundle has to be disassembled to allow SPB duplication/separation upon quiescence exit and cell cycle re-entry.

Discussion

Our results shed light on the precise temporal sequences that generate a Q-nMT bundle upon quiescence establishment in yeast. From bacteria to human stem cells, modifications of the cell physico-chemical properties are known to accompany quiescence establishment. Among these modifications, a reduction of the cellular volume increases molecular crowding (Joyner et al., 2016) and pH acidification causes changes in the surface charges of macromolecules and viscosity increases (Charruyer and Ghadially, 2018; Jacquel et al., 2021; Munder et al., 2016; Persson et al., 2020). Much evidence points to these modifications as a trigger for the auto-assembly of several types of enzyme-containing granules (Munder et al., 2016; Petrovska et al., 2014; Rabouille and Alberti, 2017), or complex structures such as P-bodies and Proteasome Storage Granules (Peters et al., 2013; Jacquel et al., 2021; Currie et al., 2023). Recently, Molines and colleagues showed that cytoplasmic viscosity modulates MT dynamics *in vivo* (Molines et al., 2022). Here, we show that Q-nMT bundle formation does not rely on modifications of the physicochemical properties that cells experience upon quiescence establishment (Sup. Fig. 1). In fact, dynamic cMTs and a stable Q-nMT bundle can be observed simultaneously in a quiescent cell (Sup. Fig. 1H), while physicochemical properties evolve in parallel both in the nucleus and in the cytoplasm (Joyner et al., 2016). Importantly, reduction of the cellular volume, pH acidification and increased viscosity are observed within minutes upon glucose starvation (Joyner et al., 2016) while the Q-nMT bundle needs a couple of days to be fully assembled (**Fig. 1A**). Further, we show that its formation cannot be delayed in time (**Fig. 1H**) and as such probably depends on an active process induced by a transient signal emitted upon glucose exhaustion. We speculate that the SPB may act as a platform that integrates this signal, and transfers it to the MT machinery in order to assemble a stable parallel structure.

As it is required for the onset of Q-nMT bundle formation (**Fig. 3B**), Aurora B/Ilp1, a kinase that plays a key role at the MT-kinetochore interface where it senses tension, could be one of the target of the above-mentioned nutritional signal. In parallel, upon quiescence establishment, chromosomes hyper-condensation (Guidi et al., 2015; Rutledge et al., 2015) may modify tension at the kinetochore/MT interface and as such could contribute to the initiation of phase I. Besides, Bim1 has also been involved in MT-kinetochore attachment (Dudziak et al., 2021; Akhmanova and Steinmetz, 2015). Although it deletion alone has no effect on Q-nMT bundle formation, its role become critical for phase I if kinetochore-MT interaction are already destabilized by the absence of other CPC components such as Sli15 and Bir1 (**Fig. 3D** and Sup. Fig. 3E). Altogether, these observations point to kinetochore-MT interaction as essential for phase I initiation, as confirmed by the absence of Q-nMT bundle in the *ndc80-1* mutant (**Fig. 3A**).

In phase I, SPB-anchored MTs elongate and are concomitantly stabilized (**Fig. 1 A-C**). This step requires the kinesin-14 Kar3 and its regulator Cik1 (**Fig. 4B**). During mating (Molodtsov et al., 2016), and in early mitosis, when half-spindles form (Kornakov et al., 2020), Kar3/Cik1, together with Bim1, align and cross-link growing MTs along existing ones, thereby promoting the organization of MTs into parallel bundles. Yet, in mitosis, the kinesin-14/EB1 complex promotes MT dynamics (Kornakov et al., 2020). In phase I, whether the robust MT stabilization depends on the modification of the kinesin-14/EB1 complex properties or is due to additional specific cross-linker(s) remains to be clarified (**Fig. 6b**).

In quiescence, deletion of either monopolin or Slk19 leads to the formation of short, shattered and flared MT structures, phenotypes that are worsened by the deletion of Bim1 (**Fig. 3F-H** and Sup. Fig. 3F). Since Monopolin and Slk19 are involved in kinetochore clustering (Plowman et al.,

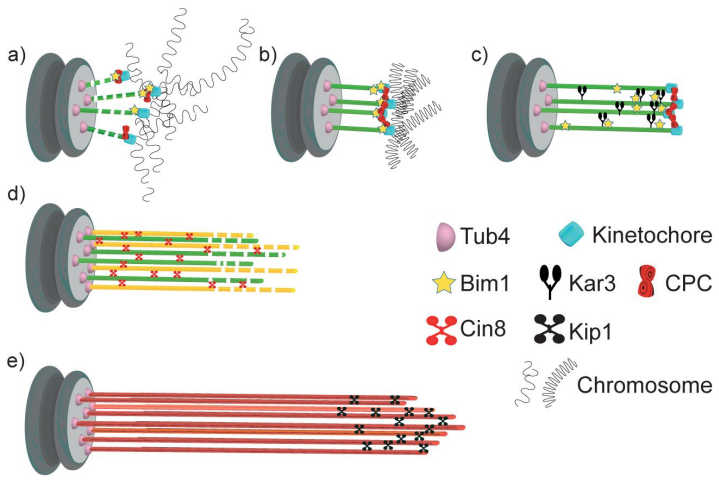

Figure 6

Model for Q-nMT bundle assembly

MT-kinetochore interaction and Ilp1 (Aurora B) are required for the onset of phase I. Kar3 (kinesin-14) and its regulator Cik1 are essential to initiate Q-nMT bundle elongation. Although deletion of *BIM1* (EB1) has no effect, it becomes critical for phase I if kinetochore-MT interactions are already destabilized by the absence of Chromosome Passenger Complex components. Kinetochore clustering by the monopolin complex and Slk19 is needed to maintain MT bundling while phase I MTs elongate. During phase I, Tub4 (ɣ-Tubulin) accumulates at the SPB. In phase II, a second wave of MT nucleation and elongation occur. Phase II MTs are concurrently stabilized along pre-existing phase I MTs, in a Cin8 (kinesin-5)-dependent manner. Phase I and phase II MTs + end (>1 µm) remain dynamic until the full length Q-nMT bundle stabilization is reached via the action of Kip1 (kinesin-5), about 2 days after glucose exhaustion.

2019; Rabitsch et al., 2003; Tóth et al., 2000; Lee et al., 2004; Mittal et al., 2019; Movshovich et al., 2008; Richmond et al., 2013; Zeng et al., 1999), we speculate that kinetochore-kinetochore interaction may not only help preventing depolymerization of single MT, but also constrain elongating phase I MTs and facilitate their concomitant cross-linking (**Fig. 6c**).

With the initiation of phase I, Tub4 starts accumulating at the SPB to allow the second wave of MT nucleation observed in phase II. When phase II MTs elongate, they are concurrently stabilized along pre-existing phase I MTs (**Fig. 6d**). This step relies on the kinesin-5/Cin8 as Q-nMT bundles assembled in *cin8Δ* cells are thinner than WT Q-nMT bundles (**Fig. 4C and D**). Intriguingly, *in vitro*, the monomeric form of the vertebrate kinesin-5 Eg5 promotes MT nucleation and stabilizes lateral tubulin-tubulin contacts (Chen et al 2019). We thus assume that in the absence of Cin8, either nucleation of phase II MTs cannot occur, or phase II MTs can elongate, but cannot be cross-linked and stabilized to phase I MT while they grow, and as such rapidly vanish. An absence of bundle thickening in phase II is also observed in the "*Tub1-only*" mutant *i.e.* in the absence of Tub3. Tubulin isoforms or tubulin PTM can allow the recruitment of specific kinesins and thereby modify MT properties, see for example (Sirajuddin et al., 2014; Peris et al., 2009; Dunn et al., 2008). May Tub3 be important for Cin8 recruitment or function during phase II?

Then, MTs elongate, but their distal parts (>1 µm) are not yet stable (**Fig. 1A**). The full-length Q-nMT bundle stabilization is reached about 2 days after glucose exhaustion. This step depends on the kinesin-5/Kip1 (**Fig. 4 G-H** and Sup. Fig. 4E) that is essential to cross-link and stabilize elongating MTs during phase III (**Fig. 6e**). Accordingly, we observed a Kip1 enrichment at the Q-nMT bundle +ends (**Fig. 4F**). Thus, in agreement with their ability to form homo-tetramers able to cross-link (Acar et al., 2013; Kapitein et al., 2005; Scholey et al., 2014; Weinger et al., 2011) and stabilize parallel MTs (Kapitein et al., 2005; Shimamoto et al., 2015; Yukawa et al., 2020), the two yeast kinesin 5 are essential for Q-nMT bundle formation. Yet, in quiescence, just as in mitosis, Kip1 and Cin8 have clearly non-equivalent functions (Roostalu et al., 2011; Shapira and Gheber, 2016).

So far, our results indicate that the Q-nMT bundle formation mechanism is different from the one at work during mitotic spindle assembly. Similarly, we show that Q-nMT bundle disassembly relies on a mechanism that does not involves the same pathway than mitotic spindle dismantlement. Indeed, Q-nMT bundle disassembly involves Kip3 (**Fig. 5C-D**) but is independent of the anaphase-promoting complex and Aurora B (Woodruff et al., 2010). Interestingly, the longest MTs start depolymerizing from their +ends first. Then, when they reach the +ends of shorter MTs, they embark them on depolymerization (Sup. Fig. 5A). This cooperative behavior has been observed *in vitro* within parallel MT bundles (Laan et al., 2008) and our data indicate that such a comportment can exist *in vivo*. In telophase, the CPC localizes to the end of the two half-spindles in order to participate in mitotic spindle disassembly (Ibarlucea-Benitez et al., 2018). Intriguingly, in quiescence, CPC is poised at the Q-nMT bundle + end (**Fig. 3C**). May this CPC localization facilitate Q-nMT bundle rapid disassembly once environmental conditions become favorable, thus ensuring quiescence exit efficiency?

Finally, in the present study, we show that the Q-nMT bundle is required for WT cells survival in quiescence. While we do not yet know why this structure is important to face chronological age, it is clear that the presence of Q-nMT bundle strongly alters the nuclear organization (Laporte et al., 2013; Laporte and Sagot, 2014; Laporte et al., 2016). As chromatin organization influences gene expression, one hypothesis could be that the presence of Q-nMT bundle is required for expression of genes required for cell survival in quiescence. Another attractive hypothesis could be that the Q-nMT bundle is the yeast analog of the primary cilium of mammalian cells. In fact, these two structures formed upon proliferation cessation, they are both composed of highly stable parallel MTs, their formation involve MT motors, and they are both template from the centriole/SPB. More importantly, we show here that the Q-nMT disassembly is needed to authorize

nascent SPB separation upon quiescence exit (**Fig. 5**). Thus, the Q-nMT bundle disassembly may controls reentry into the proliferation cycle, just as the primary cilium does in ciliated mammalian cells (Goto et al., 2017; Kim and Tsiokas, 2011).

Materiel and Methods

Yeast strains, plasmids and growth conditions

All the strains used in this study are isogenic to BY4741 (*mat a, leu2Δ0, his3Δ0, ura3Δ0, met15Δ0)* or BY4742 (*mat alpha, leu2Δ0, his3Δ0, ura3Δ0, lys2Δ0),* available from GE Healthcare Dharmacon Inc. (UK), except in **Fig. 2**, in which S288c strains were used (Nsamba et al., 2021). BY strains carrying GFP fusions were obtained from ThermoFisher Scientific (Waltham, MA, USA). Integrative plasmid p*Tub1-mTurquoise2-Tub1*, p*Tub1-wasabi-Tub1*, p*Tub1-mRUBY2-Tub1*, p*Tub1-mEOS2-Tub1* were a generous gift of Wei-Lih Lee (Markus et al., 2015). The strain expressing SPC42-mRFP1 is a generous gift from E. O'Shea (Huh et al., 2003). The strain expressing TUB4-mTQZ is generous gift of S. Jaspersen (Burns et al., 2015). Three copies of eGFP in tandem were integrated at the 3' end of *DAD2*, *TUB3* or *KAR3* endogenous loci respectively. Plasmids for expressing Nup2-RFP (p3695) or Bim1-3xGFP (p4587) from the endogenous locus were described in (Laporte et al., 2013).

For **Fig. 1F**, *pHIS3:mTurquoise2-Tub1+3'UTR::LEU2* was integrated at *TUB1* locus, then a pRS303-*ADH2p-mRuby2-Tub1* was integrated at the *HIS3* locus. To generate this plasmid, the *ADH2* promoter was amplified from yeast genomic DNA flanked with NotI and SpeI restrictions sites and inserted in pRS303. The mRuby2-Tub1+3'UTR, including the 116-nucleotide intron and 618 nucleotides downstream the stop codon was cloned between SpeI/SalI sites.

Yeast cells were grown in liquid YPDA medium at 30 °C in flasks as described previously in (Sagot et al., 2006) except for experiments using thermosensitive strains, where cells were first grown at 25 °C then shifted at 37 °C for indicated time before imaging.

Experiment in Sup. Fig. 1I was performed as described in (Orij et al., 2009, Peters et al., 2013). In brief, proliferating cells were transfered at an OD_{600nm} of 0.5 in Hepes buffer (25 mM Hepes, pH 7.4, 200 mM KCl, 1 mM $CaCl_2$, and 2% dextrose) buffered either at pH 4 or 7.5, in the presence of 100 µM CCCP (Sigma-Aldrich). After 150 min 30 °C shaking, cells were imaged (for mTQZ-Tub1) or fixed and stained using Alexa Fluor 568–phalloidin (Invitrogen) as described (Sagot et al., 2006).

For live cell imaging, 2 µL of the cell culture were spotted onto a glass slide and immediately imaged at room temperature.

For quiescence exit, cells were then incubated 2-3 min in liquid YPD and a 2 µL were spread onto a 2 % agarose microscope pad containing YPD. Individual cells were imaged every hour, up to 6 or 12 h at 21°C. For quiescence exit in presence of cycloheximide (**Fig. 5A**), cells were pre-incubated 30 min in the presence of the drug prior quiescence exit. Cycloheximide was used at 180 µM (Sigma-Aldrich), Nocodazole was used at 30 µg/mL (7.5 µM) (Sigma-Aldrich).

Fluorescence Microscopy

Cells were observed on a fully-automated Zeiss 200M inverted microscope (Carl Zeiss, Thornwood, NY, USA) equipped with an MS-2000 stage (Applied Scientific Instrumentation, Eugene, OR, USA), a Lambda LS 300 Watt xenon light source (Sutter, Novato, CA, USA), a 100X 1.4NA Plan-Apochromat objective, and a 5 position filter turret. For RFP imaging we used a Cy3 filter (Ex: HQ535/50 nm – Em: HQ610/75 nm – BS: Q565 nm lp). For GFP imaging, we used a FITC filter (excitation, HQ487/25 nm; emission, HQ535/40 nm; beam splitter, Q505 nm lp). For mTurquoise imaging we used a DAPI filter (Ex: 360/40 nm – Em: 460/50 nm– BS: 400 nm). All the filters are from Chroma Technology

Corp. Images were acquired using a CoolSnap HQ camera (Roper Scientific, Tucson, AZ, USA). The microscope, camera, and shutters (Uniblitz, Rochester, NY, USA) were controlled by SlideBook software 5. 0. (Intelligent Imaging Innovations, Denver, CO, USA).

For PALM (**Fig. 4E**) a Nikon Ti-Eclipse equipped with iLas2 TIRF arm, laser diodes (405, 488, 532, 561, 642 nm), a 100x 1.49 oil (TIRF) objective connected to a EMCCD Camera Photometrics Evolve was used.

Immunofluorescence was done as in (Laporte et al. 2015), using AlexaFluor Phalloidin (Invitrogen).

For expansion microscopy (Sup **Fig. 2A**), spheroplasts were obtained as described in (Laporte et al., 2016). After washes in 10 mg/mL NaBH4 in PEMS for 10 min, spheroplasts were seeded on 12 mm round poly-L-lysine coated coverslips, washed twice for 30 min in 100 µL PEM-BAL (PEM + 1% BSA) and incubated with the primary antibodies (anti-GFP from mouse; Roche, ref. 11814460001, 1/50; anti-alpha-tubulin from rat; YOL1/34, Abcam, ref. Ab6161, 1/100) for 1 hour at 37°C. Cells were then washed three times in PEM-BAL and incubated with the secondary antibodies (Goat anti-mouse AlexaFluor®488 1/200 and Donkey anti-rat AlexaFluor®555; A11029 and A21434 respectively, ThermoFisher Scientific, Waltham, MA) for 45 min at 37 °C. Cells were then washed three times with PBS. Cells were processed for Expansion Microscopy as previously described in (Bahri et al., 2021). Spheroplasts were incubated for 10 min in 0.25 % GA in PBS, washed in PBS three times for 5 min, and processed for gelation. A drop of 100 µL of ExM MS (8.625% (wt/wt) SA, 2.5% (wt/wt) AA, 0.15 % (wt/wt) BIS, 2 M NaCl in 1× PBS) was placed on the chilled Parafilm, and coverslips were put on the drop with cells facing the solution and incubated for 3 min. Then the coverslips were transferred to a 35 µL of ExM MS supplemented with 0.2 % APS and 0.2 % TEMED, with the initiator (APS) added last. Gelation proceeded for 3 min on ice, and samples were incubated at 37 °C in a humidified chamber in the dark for 1 h. Then coverslips with attached gels were transferred into a six-well plate for incubation in 2 mL of digestion buffer (1× TAE buffer, 0.5% Triton X-100, 0.8 M guanidine hydrochloride, pH ~8.3) supplemented with DAPI (1 µg/mL) for 10-15 min at 37 °C, until the gels detached. Fresh proteinase K at 8 units/mL was then added and samples incubated at 37 °C for 30 min. Finally, gels were removed and placed in 10mL petri dishes filled with ddH2O for expansion. Water was exchanged at least twice every 30 min, and incubated in ddH2O overnight at RT. Gels expanded between 4× and 4.2× according to SA purity. Expanded cells were imaged with a UPlanS Apo 100×/1.4 oil immersion objective in an Olympus IX81 microscope (Olympus, Tokyo, Japan). For Structured illumination microscopy (SIM, Fig. 7D), a ZEISS Lattice Lightsheet 7 was used.

Laser ablation (**Fig. 3I**) was performed at room temperature with a 100X oil Plan-Apochromat objective lens (NA 1.4) and an Axio-Observed.Z1 microscope (Carl Zeiss) equipped with a spinning disk confocal (Yokogawa), an EMCCD Evolve camera (Photometrics and Roper Scientific) and 491 nm (100 mW; Cobolt calypso) and 561 nm (100 mW; Cobolt Jive) lasers. Images were acquired with Metamorph software (Roper Scientific). Every 5 to 20 s, a Z-series of 0.4 µm steps were acquired. A 355 nm microchip laser (Teem Photonics) with a 21 kHz repetition rate, 0.8 µJ energy/pulse, 2 kW of peak power and 400 ps pulse width, powered with an iLas2 PULSE system (Roper Scientific) was used between 10 to 40 % power with one pulse of a spot length of 100 points. Breakage was considered as successful if a non-alignment between the two remaining Q-n MT bundle fragments was observed.

Z-stacks were deconvolved using the Deconvolution Lab plugin (**Fig. 1D**; **Fig. 3C,E,F** **Fig. 4A,F**). In **figures 1F**, **4A, B, G**, supplemental figure 1H and 3B a faint and fuzzy fluorescence signal is detected in some cell cytoplasm using the GFP filter set. This signal is not GFP but rather due to a non-specific yellow background fluorescence.

Image analysis

Distribution and associated statistics were performed using GraphPad Prism 5 (GraphPad Software, Inc. La Jolla, USA). Unless specified, histograms and scatter dot plots show the mean and the error bars indicate SD. MT length was measured on MAX-projected image using imageJ.

For MT fluorescence intensity measurement, a line scan (i1) of 4 pixel width containing both FP signal and background was drawn along MTs on SUM projection image (3-4 Z-plans) using ImageJ. A line of 8 pixels width (at the same location) was drawn in order to calculate the intensity of the surrounding background (i2). The real intensity (ir) was calculated as follow: int=(i1-((i2×8)-(i1×4))/4). Similar approach was conducted to measure Tub4 fluorescence intensity (**Fig. 1E**) *i.e.* (i1) and (i2) were two boxes, the second including the first one. Intensity was calculated as follow: int=[i1-([(i2xi2$_{surface}$)-(i1xi1$_{surface}$)]/(i2$_{surface}$-i1$_{surface}$))*i1$_{surface}$]. For morphometric Q-nMT bundle property distribution (**Fig. 1C** and **4B**)the mean fluorescence intensity was measured in each individual cell, in a finite area localized adjacent to the SPB (0,4 µm – 3-4 Z stack sum projected) as an estimate of Q-nMT bundle width and plotted as a function of the according measured bundle length.

For Nuf2 fluorescence intensity measurement at SPB (Sup. Fig. 1D), GFP and RFP line scan measurements were done on a 3-4 Z-plans sum projection. The “SPB localization zone” was defined as the length ending at the second pixel after the brightest RFP signal of Spc42-RFP. The remaining Q-nMT bundle zone was defined as the “+end zone”. The total Nuf2-GFP signal detected along the Q-nMT bundle was set to 100 % (sum projection imaged) allowing to determine the percentage of the signal measured at “SPB localization zone” and at “+end zone”

Normalized Q-nMT bundle length (**Fig. 3C**) was done after line scan intensity measurement. mTQZ-Tub1 intensities slopes were first aligned on their inflexion point. To compare Q-nMT bundle with different lengths, we first sorted Q-nMT bundle <1.8 µm. After an artificial isotropic expansion, we fit all MT structures to length order. Then, corresponding mean intensity of Q-nMT bundle (mTZQ-Tub1) and GFP signal were calculated.

To measure the Q-nMT bundle depolymerization (**Fig. 5A and E**), individual Q-nMT bundle length were measured over time. The first measurement was set at 100 % of the length, and the following percentages calculated accordingly. A fluorescence drop above or equal to 25 % defines the inflexion point of the slope, and was used to align the different length measurements. The FWHM (Full Width at Half Maximum) was calculated by measuring fluorescence intensity of a line crossing perpendicularly a Q-nMT bundle, from a sum projection. After fitting intensity level with Gaussian distribution and obtained the standard deviation (σ) value, FWHM was calculated using the equation 2√(2ln2)xσ. In **Fig. 5B**, FWHM was measured at 0.5 µm of the SPB.

Western blots

Western blots were done as described in (Sagot et al., 2006) using anti-GFP antibodies (Roche); anti-Tat1 antibodies (a generous gift from J-P. Javerzat) and antibody against the budding yeast Act1 or Sac6, generous gifts from B. Goode.

Phenotypical analysis of cells without Q-nMT bundle

WT strains were grown to glucose exhaustion (OD ~6.5), washout with “old YPDA” and pulsed with either DMSO or Nocodazole (30µg/mL) for 24 h. Cells were then washed twice in “old YPDA” before being incubated in the same medium. Dead cell measurement was done using methylene blue staining. The capacity of cells to exit quiescence was scored after cells micro-manipulation (N=4, n>100) as described in (Laporte et al., 2011).

Supplemental data

Supplementary Figure 1 further described the 3 steps of Q-nMT bundle formation. It shows the impact of physico-chemical cell properties on MT stabilization and demonstrate that Q-nMT bundle is required for both cell viability in quiescence and quiescence exit fitness.

Supplementary Figure 2 describes the impact of the alpha tubulin level on Q-nMT bundle assembly.

Supplementary Figure 3 demonstrates that kinetochore-MT interactions are not required for Q-nMT bundle maintenance and that mutants affected for kinetochore-kinetochore interactions have a reduced viability in quiescence.

Supplementary Figure 4 impact of various yeast kinesin deletion on Q-nMT bundle morphometric parameters.

Supplementary Figure 5 Q-nMT bundle disassembly in mutants affected for mitotic spindle dismantlement.

Acknowledgements

The authors would like to thank the Bordeaux Imaging center for the help in super-resolution imaging. We also thank Zeiss for their help with SIM. We express our gratitude to E. O'Shea, S. Jaspersen, J-P. Javerzat, Wei-Lih Lee and B. Goode for sharing reagents. We would like to thank J-P. Javerzat for helpful and constructive discussions about our work. DL, AML, JD and IS were supported by a grant from the ANR-21-CE13-0023-01, a Ligue Contre le Cancer Régionale – Dordogne grant #193366 and the CNRS. MG and EN were supported by a National Science Foundation grant number MCB-1846262. AR was supported by the Conseil Régional d'Aquitaine (#20111301010) and the CNRS.

Author Contributions

D. Laporte did all the experiments described in this manuscript, except **Fig. 1F**, **1H**, **Fig. 5 G-H** and Sup. Fig. 5G to I that were performed by A. Massoni-Laporte, together with all image deconvolution, and **Fig. 4E** and Sup. Fig. 2A and 3A that were done by J. Dompierre. A. Royou helped for pulse-laser experiments of **Fig. 3I** and Sup **Fig. 3H-I**. C. Lefranc did molecular biology and western blots. D. Mauboules performed yeast genetic for **Fig. 2**. M. L. Gupta Jr and E. T. Nsamba created the Tub1-only mutant (**Fig. 2**). L. Gal and M. Schuldiner performed high throughput deletion screen. IS and DL designed and supervised the experiments. IS and DL wrote the manuscript.

Abbreviations

- MT
  microtubule
- SPB
  spindle pole body
- GTP
  guanosine triphosphate
- MTOC
  microtubule organizing centers

- ɣ-TuC
  ɣ-tubulin complex
- MAPs
  microtubule associated proteins
- Q-nMT bundle
  quiescence specific nuclear microtubule bundle
- CPC
  chromosome passenger complex

References

Acar S. *et al.* (2013) **The bipolar assembly domain of the mitotic motor kinesin-5** *Nat Commun* **4** https://doi.org/10.1038/ncomms2348

Aiken J., Moore J.K., Bates E.A. (2019) **TUBA1A mutations identified in lissencephaly patients dominantly disrupt neuronal migration and impair dynein activity** *Human Molecular Genetics* **28**:1227–1243 https://doi.org/10.1093/hmg/ddy416

Akhmanova A., Steinmetz M.O. (2015) **Control of microtubule organization and dynamics: two ends in the limelight** *Nature Reviews Molecular Cell Biology* **16**:711–726 https://doi.org/10.1038/nrm4084

Anvarian Z., Mykytyn K., Mukhopadhyay S., Pedersen L.B., Christensen S.T. (2019) **Cellular signalling by primary cilia in development, organ function and disease** *Nat Rev Nephrol* **15**:199–219 https://doi.org/10.1038/s41581-019-0116-9

Baas P.W., Rao A.N., Matamoros A.J., Leo L. (2016) **Stability properties of neuronal microtubules** *Cytoskeleton (Hoboken* **73**:442–460 https://doi.org/10.1002/cm.21286

Bahri H. *et al.* (2021) **TMEM70 forms oligomeric scaffolds within mitochondrial cristae promoting in situ assembly of mammalian ATP synthase proton channel** *Biochim Biophys Acta Mol Cell Res* **1868** https://doi.org/10.1016/j.bbamcr.2020.118942

Bergman Z.J., Xia X., Amaro I.A., Huffaker T.C. (2012) **Constitutive dynein activity in She1 mutants reveals differences in microtubule attachment at the yeast spindle pole body** *Mol Biol Cell* **23**:2319–2326 https://doi.org/10.1091/mbc.E12-03-0223

Bodakuntla S., Jijumon A.S., Villablanca C., Gonzalez-Billault C., Janke C. (2019) **Microtubule-Associated Proteins: Structuring the Cytoskeleton** *Trends Cell Biol* **29**:804–819 https://doi.org/10.1016/j.tcb.2019.07.004

Bode C.J., Gupta M.L., Suprenant K.A., Himes R.H. (2003) **The two alpha-tubulin isotypes in budding yeast have opposing effects on microtubule dynamics in vitro** *EMBO Rep* **4**:94–99 https://doi.org/10.1038/sj.embor.embor716

Bodrug T. *et al.* (2020) **The kinesin-5 tail domain directly modulates the mechanochemical cycle of the motor domain for anti-parallel microtubule sliding** *eLife* **9** https://doi.org/10.7554/eLife.51131

Burns S., Avena J.S., Unruh J.R., Yu Z., Smith S.E., Slaughter B.D., Winey M., Jaspersen S.L. (2015) **Structured illumination with particle averaging reveals novel roles for yeast centrosome components during duplication** *Elife* **4** https://doi.org/10.7554/eLife.08586

Cairo G., Lacefield S. (2020) **Establishing correct kinetochore-microtubule attachments in mitosis and meiosis** *Essays in Biochemistry* **64**:277–287 https://doi.org/10.1042/EBC20190072

Charruyer A., Ghadially R. (2018) **Influence of pH on Skin Stem Cells and Their Differentiation** *Curr Probl Dermatol* **54**:71–78 https://doi.org/10.1159/000489520

Cheeseman I.M., Chappie J.S., Wilson-Kubalek E.M., Desai A. (2006) **The conserved KMN network constitutes the core microtubule-binding site of the kinetochore** *Cell* **127**:983–997 https://doi.org/10.1016/j.cell.2006.09.039

Chen G.-Y., Cleary J.M., Asenjo A.B., Chen Y., Mascaro J.A., Arginteanu D.F.J., Sosa H., Hancock W.O. (2019) **Kinesin-5 Promotes Microtubule Nucleation and Assembly by Stabilizing a Lattice-Competent Conformation of Tubulin** *Curr Biol* **29**:2259–2269 https://doi.org/10.1016/j.cub.2019.05.075

Cleary J.M., Hancock W.O. (2021) **Molecular mechanisms underlying microtubule growth dynamics** *Curr Biol* **31**:R560–R573 https://doi.org/10.1016/j.cub.2021.02.035

Corbett K.D., Yip C.K., Ee L.-S., Walz T., Amon A., Harrison S.C. (2010) **The monopolin complex crosslinks kinetochore components to regulate chromosome-microtubule attachments** *Cell* **142**:556–567 https://doi.org/10.1016/j.cell.2010.07.017

Currie S.L., Xing W., Muhlrad D., Decker C.J., Parker R., Rosen M.K. (2023) **Quantitative reconstitution of yeast RNA processing bodies** *Proc Natl Acad Sci U S A* **120** https://doi.org/10.1073/pnas.2214064120

DeLuca K.F., Meppelink A., Broad A.J., Mick J.E., Peersen O.B., Pektas S., Lens S.M.A., DeLuca J.G. (2018) **Aurora A kinase phosphorylates Hec1 to regulate metaphase kinetochore-microtubule dynamics** *J Cell Biol* **217**:163–177 https://doi.org/10.1083/jcb.201707160

Dudziak A., Engelhard L., Bourque C., Klink B.U., Rombaut P., Kornakov N., Jänen K., Herzog F., Gatsogiannis C., Westermann S. (2021) **Phospho-regulated Bim1/EB1 interactions trigger Dam1c ring assembly at the budding yeast outer kinetochore** *EMBO J* **40** https://doi.org/10.15252/embj.2021108004

Dunn S., Morrison E.E., Liverpool T.B., Molina-París C., Cross R.A., Alonso M.C., Peckham M. (2008) **Differential trafficking of Kif5c on tyrosinated and detyrosinated microtubules in live cells** *J Cell Sci* **121**:1085–1095 https://doi.org/10.1242/jcs.026492

Fridman V., Gerson-Gurwitz A., Shapira O., Movshovich N., Lakämper S., Schmidt C.F., Gheber L. (2013) **Kinesin-5 Kip1 is a bi-directional motor that stabilizes microtubules and tracks their plus-ends in vivo** *J Cell Sci* **126**:4147–4159 https://doi.org/10.1242/jcs.125153

Fukuda Y., Luchniak A., Murphy E.R., Gupta M.L. (2014) **Spatial control of microtubule length and lifetime by opposing stabilizing and destabilizing functions of Kinesin-8** *Curr Biol* **24**:1826–1835 https://doi.org/10.1016/j.cub.2014.06.069

Goodson H.V., Jonasson E.M. (2018) **Microtubules and Microtubule-Associated Proteins** *Cold Spring Harb Perspect Biol* **10** https://doi.org/10.1101/cshperspect.a022608

Goto H., Inaba H., Inagaki M. (2017) **Mechanisms of ciliogenesis suppression in dividing cells** *Cell Mol Life Sci* **74**:881–890 https://doi.org/10.1007/s00018-016-2369-9

Gudimchuk N.B., McIntosh J.R. (2021) **Regulation of microtubule dynamics, mechanics and function through the growing tip** *Nat Rev Mol Cell Biol* **22**:777–795 https://doi.org/10.1038/s41580-021-00399-x

Guidi M., Ruault M., Marbouty M., Loïodice I., Cournac A., Billaudeau C., Hocher A., Mozziconacci J., Koszul R., Taddei A. (2015) **Spatial reorganization of telomeres in long-lived quiescent cells** *Genome Biol* **16** https://doi.org/10.1186/s13059-015-0766-2

Hahn I., Voelzmann A., Liew Y.-T., Costa-Gomes B., Prokop A. (2019) **The model of local axon homeostasis - explaining the role and regulation of microtubule bundles in axon maintenance and pathology** *Neural Dev* **14** https://doi.org/10.1186/s13064-019-0134-0

Heald R., Khodjakov A. (2015) **Thirty years of search and capture: The complex simplicity of mitotic spindle assembly** *J Cell Biol* **211**:1103–1111 https://doi.org/10.1083/jcb.201510015

Hibbel A., Bogdanova A., Mahamdeh M., Jannasch A., Storch M., Schäffer E., Liakopoulos D., Howard J. (2015) **Kinesin Kip2 enhances microtubule growth in vitro through length-dependent feedback on polymerization and catastrophe** *Elife* **4** https://doi.org/10.7554/eLife.10542

Huh W.-K., Falvo J.V., Gerke L.C., Carroll A.S., Howson R.W., Weissman J.S., O'Shea E.K. (2003) **Global analysis of protein localization in budding yeast** *Nature* **425**:686–691 https://doi.org/10.1038/nature02026

Ibarlucea-Benitez I., Ferro L.S., Drubin D.G., Barnes G. (2018) **Kinesins relocalize the chromosomal passenger complex to the midzone for spindle disassembly** *J Cell Biol* **217**:1687–1700 https://doi.org/10.1083/jcb.201708114

Jacquel B., Aspert T., Laporte D., Sagot I., Charvin G. (2021) **Monitoring single-cell dynamics of entry into quiescence during an unperturbed life cycle** *Elife* **10** https://doi.org/10.7554/eLife.73186

Janke C., Magiera M.M. (2020) **The tubulin code and its role in controlling microtubule properties and functions** *Nat Rev Mol Cell Biol* **21**:307–326 https://doi.org/10.1038/s41580-020-0214-3

Jin Q., Trelles-Sticken E., Scherthan H., Loidl J. (1998) **Yeast nuclei display prominent centromere clustering that is reduced in nondividing cells and in meiotic prophase** *J. Cell Biol* **141**:21–29

Joyner R.P., Tang J.H., Helenius J., Dultz E., Brune C., Holt L.J., Huet S., Müller D.J., Weis K. (2016) **A glucose-starvation response regulates the diffusion of macromolecules** *Elife* **5** https://doi.org/10.7554/eLife.09376

Kapitein L.C., Peterman E.J.G., Kwok B.H., Kim J.H., Kapoor T.M., Schmidt C.F. (2005) **The bipolar mitotic kinesin Eg5 moves on both microtubules that it crosslinks** *Nature* **435**:114–118 https://doi.org/10.1038/nature03503

Kim S., Tsiokas L. (2011) **Cilia and cell cycle re-entry: more than a coincidence** *Cell Cycle* **10**:2683–2690 https://doi.org/10.4161/cc.10.16.17009

Kirschner M., Mitchison T. (1986) **Beyond self-assembly: from microtubules to morphogenesis** *Cell* **45**:329–342

Kornakov N., Möllers B., Westermann S. (2020) **The EB1-Kinesin-14 complex is required for efficient metaphase spindle assembly and kinetochore bi-orientation** *J Cell Biol* **219** https://doi.org/10.1083/jcb.202003072

Laan L., Husson J., Munteanu E.L., Kerssemakers J.W.J., Dogterom M. (2008) **Force-generation and dynamic instability of microtubule bundles** *Proc Natl Acad Sci U S A* **105**:8920–8925 https://doi.org/10.1073/pnas.0710311105

Laporte D., Courtout F., Pinson B., Dompierre J., Salin B., Brocard L., Sagot I. (2015) **A stable microtubule array drives fission yeast polarity reestablishment upon quiescence exit** *J. Cell Biol* **210**:99–113 https://doi.org/10.1083/jcb.201502025

Laporte D., Courtout F., Salin B., Ceschin J., Sagot I. (2013) **An array of nuclear microtubules reorganizes the budding yeast nucleus during quiescence** *J. Cell Biol* **203**:585–594 https://doi.org/10.1083/jcb.201306075

Laporte D., Courtout F., Tollis S., Sagot I. (2016) **Quiescent Saccharomyces cerevisiae forms telomere hyperclusters at the nuclear membrane vicinity through a multifaceted mechanism involving Esc1, the Sir complex, and chromatin condensation** *Mol. Biol. Cell* **27**:1875–1884 https://doi.org/10.1091/mbc.E16-01-0069

Laporte D., Sagot I. (2014) **Microtubules move the nucleus to quiescence** *Nucleus* **5**:113–118 https://doi.org/10.4161/nucl.28538

Lee B.H., Kiburz B.M., Amon A. (2004) **Spo13 maintains centromeric cohesion and kinetochore coorientation during meiosis I** *Curr Biol* **14**:2168–2182 https://doi.org/10.1016/j.cub.2004.12.033

Liu P., Würtz M., Zupa E., Pfeffer S., Schiebel E. (2021) **Microtubule nucleation: The waltz between γ-tubulin ring complex and associated proteins** *Curr Opin Cell Biol* **68**:124–131 https://doi.org/10.1016/j.ceb.2020.10.004

Manning B.D., Barrett J.G., Wallace J.A., Granok H., Snyder M. (1999) **Differential regulation of the Kar3p kinesin-related protein by two associated proteins, Cik1p and Vik1p** *J Cell Biol* **144**:1219–1233 https://doi.org/10.1083/jcb.144.6.1219

Markus S.M., Omer S., Baranowski K., Lee W.-L. (2015) **Improved Plasmids for Fluorescent Protein Tagging of Microtubules in Saccharomyces cerevisiae** *Traffic* **16**:773–786 https://doi.org/10.1111/tra.12276

Meiring J.C.M., Shneyer B.I., Akhmanova A. (2020) **Generation and regulation of microtubule network asymmetry to drive cell polarity** *Curr Opin Cell Biol* **62**:86–95 https://doi.org/10.1016/j.ceb.2019.10.004

Mieck C., Molodtsov M.I., Drzewicka K., van der Vaart B., Litos G., Schmauss G., Vaziri A., Westermann S. (2015) **Non-catalytic motor domains enable processive movement and functional diversification of the kinesin-14 Kar3** *eLife* **4** https://doi.org/10.7554/eLife.04489

Mitchison T., Kirschner M. (1984) **Dynamic instability of microtubule growth** *Nature* **312**:237–242

Mittal P., Chavan A., Trakroo D., Shah S., Ghosh S.K. (2019) **Outer kinetochore protein Dam1 promotes centromere clustering in parallel with Slk19 in budding yeast** *Chromosoma* **128**:133–148 https://doi.org/10.1007/s00412-019-00694-9

Molines A.T. *et al.* (2022) **Physical properties of the cytoplasm modulate the rates of microtubule polymerization and depolymerization** *Developmental Cell* **57**:466–479 https://doi.org/10.1016/j.devcel.2022.02.001

Molodtsov M.I., Mieck C., Dobbelaere J., Dammermann A., Westermann S., Vaziri A. (2016) **A Force-Induced Directional Switch of a Molecular Motor Enables Parallel Microtubule Bundle Formation** *Cell* **167**:539–552 https://doi.org/10.1016/j.cell.2016.09.029

Movshovich N., Fridman V., Gerson-Gurwitz A., Shumacher I., Gertsberg I., Fich A., Hoyt M.A., Katz B., Gheber L. (2008) **Slk19-dependent mid-anaphase pause in kinesin-5-mutated cells** *J Cell Sci* **121**:2529–2539 https://doi.org/10.1242/jcs.022996

Munder M.C. *et al.* (2016) **A pH-driven transition of the cytoplasm from a fluid- to a solid-like state promotes entry into dormancy** *eLife* **5** https://doi.org/10.7554/eLife.09347

Muroyama A., Lechler T. (2017) **Microtubule organization, dynamics and functions in differentiated cells** *Development* **144**:3012–3021 https://doi.org/10.1242/dev.153171

Nsamba E.T., Bera A., Costanzo M., Boone C., Gupta Jr M.L. (2021) **Tubulin isotypes optimize distinct spindle positioning mechanisms during yeast mitosis** *Journal of Cell Biology* **220** https://doi.org/10.1083/jcb.202010155

Pandey H., Popov M., Goldstein-Levitin A., Gheber L. (2021) **Mechanisms by Which Kinesin-5 Motors Perform Their Multiple Intracellular Functions** *Int J Mol Sci* **22** https://doi.org/10.3390/ijms22126420

Peris L., Wagenbach M., Lafanechère L., Brocard J., Moore A.T., Kozielski F., Job D., Wordeman L., Andrieux A. (2009) **Motor-dependent microtubule disassembly driven by tubulin tyrosination** *J Cell Biol* **185**:1159–1166 https://doi.org/10.1083/jcb.200902142

Persson L.B., Ambati V.S., Brandman O. (2020) **Cellular Control of Viscosity Counters Changes in Temperature and Energy Availability** *Cell* **183**:1572–1585 https://doi.org/10.1016/j.cell.2020.10.017

Peters L.Z., Hazan R., Breker M., Schuldiner M., Ben-Aroya S. (2013) **Formation and dissociation of proteasome storage granules are regulated by cytosolic pH** *J. Cell Biol* **201**:663–671 https://doi.org/10.1083/jcb.201211146

Petrovska I. *et al.* (2014) **Filament formation by metabolic enzymes is a specific adaptation to an advanced state of cellular starvation** *Elife* https://doi.org/10.7554/eLife.02409

Plowman R. *et al.* (2019) **The molecular basis of monopolin recruitment to the kinetochore** *Chromosoma* **128**:331–354 https://doi.org/10.1007/s00412-019-00700-0

Rabitsch K.P., Petronczki M., Javerzat J.P., Genier S., Chwalla B., Schleiffer A., Tanaka T.U., Nasmyth K. (2003) **Kinetochore recruitment of two nucleolar proteins is required for homolog segregation in meiosis I** *Dev Cell* **4**:535–548 https://doi.org/10.1016/s1534-5807(03)00086-8

Rabouille C., Alberti S. (2017) **Cell adaptation upon stress: the emerging role of membrane-less compartments** *Curr Opin Cell Biol* **47**:34–42 https://doi.org/10.1016/j.ceb.2017.02.006

Richmond D., Rizkallah R., Liang F., Hurt M.M., Wang Y. (2013) **Slk19 clusters kinetochores and facilitates chromosome bipolar attachment** *Mol Biol Cell* **24**:566–577 https://doi.org/10.1091/mbc.E12-07-0552

Roll-Mecak A (2020) **The Tubulin Code in Microtubule Dynamics and Information Encoding** *Dev Cell* **54**:7–20 https://doi.org/10.1016/j.devcel.2020.06.008

Roostalu J., Hentrich C., Bieling P., Telley I.A., Schiebel E., Surrey T. (2011) **Directional Switching of the Kinesin Cin8 Through Motor Coupling** *Science* https://doi.org/10.1126/science.1199945

Roostalu J., Surrey T. (2017) **Microtubule nucleation: beyond the template** *Nat. Rev. Mol. Cell Biol* https://doi.org/10.1038/nrm.2017.75

Röper K (2020) **Microtubules enter centre stage for morphogenesis** *Philos Trans R Soc Lond B Biol Sci* **375** https://doi.org/10.1098/rstb.2019.0557

Rutledge M.T., Russo M., Belton J.-M., Dekker J., Broach J.R. (2015) **The yeast genome undergoes significant topological reorganization in quiescence** *Nucleic Acids Res* **43**:8299–8313 https://doi.org/10.1093/nar/gkv723

Sagot I., Pinson B., Salin B., Daignan-Fornier B. (2006) **Actin bodies in yeast quiescent cells: an immediately available actin reserve?** *Mol. Biol. Cell* **17**:4645–4655 https://doi.org/10.1091/mbc.E06-04-0282

Sanchez A.D., Feldman J.L. (2017) **Microtubule-organizing centers: from the centrosome to non-centrosomal sites** *Curr. Opin. Cell Biol* **44**:93–101 https://doi.org/10.1016/j.ceb.2016.09.003

Schatz P.J., Solomon F., Botstein D. (1986) **Genetically essential and nonessential alpha-tubulin genes specify functionally interchangeable proteins** *Mol Cell Biol* **6**:3722–3733 https://doi.org/10.1128/mcb.6.11.3722-3733.1986

Scholey J.E., Nithianantham S., Scholey J.M., Al-Bassam J. (2014) **Structural basis for the assembly of the mitotic motor Kinesin-5 into bipolar tetramers** *Elife* **3** https://doi.org/10.7554/eLife.02217

Shapira O., Gheber L. (2016) **Motile properties of the bi-directional kinesin-5 Cin8 are affected by phosphorylation in its motor domain** *Sci Rep* **6** https://doi.org/10.1038/srep25597

Shimamoto Y., Forth S., Kapoor T.M. (2015) **Measuring Pushing and Braking Forces Generated by Ensembles of Kinesin-5 Crosslinking Two Microtubules** *Dev Cell* **34**:669–681 https://doi.org/10.1016/j.devcel.2015.08.017

Singh S.K., Pandey H., Al-Bassam J., Gheber L. (2018) **Bidirectional motility of kinesin-5 motor proteins: structural determinants, cumulative functions and physiological roles** *Cell. Mol. Life Sci* **75**:1757–1771 https://doi.org/10.1007/s00018-018-2754-7

Sirajuddin M., Rice L.M., Vale R.D. (2014) **Regulation of microtubule motors by tubulin isotypes and post-translational modifications** *Nat Cell Biol* **16**:335–344 https://doi.org/10.1038/ncb2920

Thawani A., Petry S. (2021) **Molecular insight into how γ-TuRC makes microtubules** *J Cell Sci* **134** https://doi.org/10.1242/jcs.245464

Thomas G.E. *et al.* (2016) **EB1 regulates attachment of Ska1 with microtubules by forming extended structures on the microtubule lattice** *Nat Commun* **7** https://doi.org/10.1038/ncomms11665

Tóth A., Rabitsch K.P., Gálová M., Schleiffer A., Buonomo S.B., Nasmyth K. (2000) **Functional genomics identifies monopolin: a kinetochore protein required for segregation of homologs during meiosis i** *Cell* **103**:1155–1168 https://doi.org/10.1016/s0092-8674(00)00217-8

Weinger J.S., Qiu M., Yang G., Kapoor T.M. (2011) **A nonmotor microtubule binding site in kinesin-5 is required for filament crosslinking and sliding** *Curr Biol* **21**:154–160 https://doi.org/10.1016/j.cub.2010.12.038

Wheway G., Nazlamova L., Hancock J.T. (2018) **Signaling through the Primary Cilium** *Frontiers in Cell and Developmental Biology* **6**

Wigge P.A., Jensen O.N., Holmes S., Souès S., Mann M., Kilmartin J.V. (1998) **Analysis of the Saccharomyces spindle pole by matrix-assisted laser desorption/ionization (MALDI) mass spectrometry** *J. Cell Biol* **141**:967–977

Winey M., Bloom K. (2012) **Mitotic spindle form and function** *Genetics* **190**:1197–1224 https://doi.org/10.1534/genetics.111.128710

Woodruff J.B., Drubin D.G., Barnes G. (2010) **Mitotic spindle disassembly occurs via distinct subprocesses driven by the anaphase-promoting complex, Aurora B kinase, and kinesin-8** *J Cell Biol* **191**:795–808 https://doi.org/10.1083/jcb.201006028

Yukawa M., Teratani Y., Toda T. (2020) **How Essential Kinesin-5 Becomes Non-Essential in Fission Yeast: Force Balance and Microtubule Dynamics Matter** *Cells* **9** https://doi.org/10.3390/cells9051154

Zeng X., Kahana J.A., Silver P.A., Morphew M.K., McIntosh J.R., Fitch I.T., Carbon J., Saunders W.S. (1999) **Slk19p is a centromere protein that functions to stabilize mitotic spindles** *J Cell Biol* **146**:415–425 https://doi.org/10.1083/jcb.146.2.415

Article and author information

Damien Laporte
Univ. Bordeaux, CNRS, IBGC, UMR 5095, Bordeaux, France
For correspondence: Damien.laporte@ibgc.cnrs.fr
ORCID iD: 0000-0002-1556-5253

Aurélie Massoni-Laporte
Univ. Bordeaux, CNRS, IBGC, UMR 5095, Bordeaux, France

Charles Lefranc
Univ. Bordeaux, CNRS, IBGC, UMR 5095, Bordeaux, France

Jim Dompierre
Univ. Bordeaux, CNRS, IBGC, UMR 5095, Bordeaux, France

David Mauboules
Univ. Bordeaux, CNRS, IBGC, UMR 5095, Bordeaux, France

Emmanuel T. Nsamba
Genetics, Development, and Cell Biology, Iowa State University, Ames, IA 50011, USA

Anne Royou
Univ. Bordeaux, CNRS, IBGC, UMR 5095, Bordeaux, France

Lihi Gal
Department of Molecular Genetics, Weizmann Institute of Science, Rehovot, Israel

Maya Schuldiner
Department of Molecular Genetics, Weizmann Institute of Science, Rehovot, Israel
ORCID iD: 0000-0001-9947-115X

Mohan L. Gupta Jr
Genetics, Development, and Cell Biology, Iowa State University, Ames, IA 50011, USA

Isabelle Sagot
Univ. Bordeaux, CNRS, IBGC, UMR 5095, Bordeaux, France

Copyright

Editors

Reviewing Editor
Jens Lüders
Institute for Research in Biomedicine, Barcelona, Spain

Senior Editor
Benoît Kornmann
University of Oxford, Oxford, United Kingdom

Reviewer #1 (Public Review):

In their manuscript, Laporte et al. analyze the process of formation of the quiescent-cell nuclear microtubule (Q-nMT) bundle, a set of parallel MTs that emanate from the nuclear side of the spindle pole bodies (SPBs) upon the entry of Saccharomyces cerevisiae cells in quiescence. Based on their results, the authors propose that Q-nMT bundle formation is a multistep process that comprises three distinct sequential phases. The authors further evaluate the role of different factors during the growth of the Q-nMT bundle upon quiescence entry, as well as during the disassembly of this structure once cells resume their proliferation.

The Q-nMT is an interesting cellular structure whose physiological function is still widely unknown. Hence, providing new insights into the dynamics of Q-nMT bundle formation and identifying new factors involved in this process is an interesting topic of relevance in the field. The authors made a substantial effort in order to evaluate Q-nMT bundle formation and provide a considerable amount of data, mainly obtained from microscopy analyses. Overall, the experiments are well described and properly executed, and the data in the manuscript are clearly presented.

Despite the interest in the study, there are important issues that could affect the validity of the conclusions drawn in the manuscript. In this way, regarding the analysis of the dynamics of Q-nMT bundle formation, the experimental set up described in some of the experiments raises certain concerns, which mostly derive from the nocodazole treatments and the use of

this microtubule-depolymerizing agent as the only approach to evaluate the stability of the Q-nMT bundle. On the other hand, regarding the factors involved in Q-nMT formation, the differences in microtubule length with the wild-type strain, despite being statistically significant, are really subtle for many of the mutants analyzed (e.g., bir1, slk19, etc.). Additionally, there are proteins that are proposed to participate in the process of Q-nMT formation and whose expression during quiescence needs to be demonstrated. Finally, although the cell viability defects observed for some of the mutants in these factors could be certainly associated with the lack of expression or mutation of the specific gene under evaluation, in none of the cases can they be directly attributed to a defect in aberrant Q-nMT bundle formation.

Based on the aforementioned reasons, and despite the considerable effort by the authors, it is my impression that many of the conclusions of the manuscript are not sufficiently justified by the data provided. Additional evidence, including the incorporation of key experimental controls that are currently missing, would be required in order to more strongly support the conclusions of the manuscript.

https://doi.org/10.7554/eLife.89958.1.sa2

Reviewer #2 (Public Review):

Summary: The authors investigate the assembly of the Q-nMT, a stable microtubule structure that is assembled during quiescence. Notably, the authors show that the formation of the Q-nMT cannot be solely explained by changes in the physicochemical properties of quiescent cells. The authors report that Q-nMT assembly occurs in three regulated steps and identify kinesin motor proteins involved in the assembly and disassembly of the structure.

Strengths: The findings provide new insight into the assembly and possible function of the Q-nMT with respect to the response of haploid budding yeast to glucose starvation.

Weaknesses: The manuscript would benefit from more precise language and requires additional clarification regarding how claims are supported by the evidence. Clear definitions are also required, for example, "active process" is not defined. Some conclusions are not supported by the results, for example, the claim that the Q-nMT functions as a checkpoint effector that inhibits re-entry into the cell cycle.

https://doi.org/10.7554/eLife.89958.1.sa1

Reviewer #3 (Public Review):

In this study, the authors analyzed a unique and very stable microtubule bundle that is formed in yeast cells entering quiescence. They show that the structure is required for yeast cells to maintain viability during quiescence and that it needs to be disassembled for cell cycle re-entry. They identify different stages during the assembly process and focus on the molecular players required for microtubule bundle formation and stabilization. They identify kinetochore as well as molecular motors such as auroraB, kinesin-14, and kinesin-5 that assemble, stabilize and crosslink the microtubules of the bundle. The paper also investigates the disassembly of the structure and shows that disassembly is required for cell cycle re-entry.

The study is very comprehensive, provides quantifications to support claims, and identifies various players involved in these processes, providing mechanistic insight. It also presents various control experiments to exclude alternative explanations and support the proposed model.

It is the first molecular-level insight into how this very stable microtubule structure can be assembled, maintained, and disassembled, and how this is coordinated with cell cycle exit and re-entry. This information may be very useful when analyzing similarly stable, microtubule-based structures in other organisms such as cilia in animals, which also display cell cycle-coordinated dynamics.

Overall, this is a nicely presented study that provides important insight into the field and beyond, but there are a few points that need to be addressed regarding methods used for quantifications and data presentation.

https://doi.org/10.7554/eLife.89958.1.sa0